Ab-Initio Elasticity of the α and β Phase of Ga_2O_3

BACHELORARBEIT

zur Erlangung des akademischen Grades
Bachelor of Science
(B. Sc.)
im Fach Physik

eingereicht an der
Mathematisch-Naturwissenschaftlichen Fakultät
Institut für Physik
Humboldt-Universität zu Berlin

von
Herrn Konstantin Lion
geboren am 25.01.1993 in Berlin

Gutachter:

1. *Prof. Dr. Dr. h. c. Claudia Draxl*
2. *PD Dr. Marco Busch*

eingereicht am: *05.02.2016*

Contents

1 Introduction

Gallium oxide (Ga_2O_3), a wide-gap transparent semiconductor is a promising candidate in a number of applications, *e.g.*, as semiconducting lasers [1] and transparent electrodes for UV optoelectronic devices [2].

Depending on the preparation, it can crystallize in five different crystal structures, among them the rhombohedral α and monoclinic β phase [3]. The β phase of Ga_2O_3 is the thermodynamically stable phase at ambient conditions [4]. The unit cell has $C2/m$ symmetry [5], contains 20 atoms, and is given in Figure 1.1.

In various works, it is shown that the β phase undergoes a phase transition to

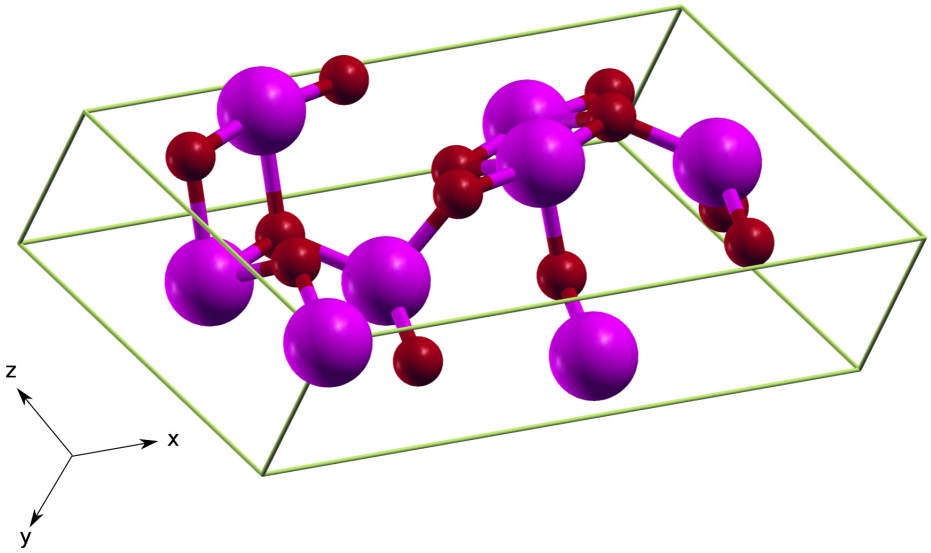

Figure 1.1: Schematic representation of the crystalline structure of the monoclinic β phase of Ga_2O_3. The unit cell has $C2/m$ symmetry and contains 4 formula units. Gallium atoms are in purple and Oxygen atoms in red.

the metastable α phase at high pressures [4, 6]. The α phase crystallizes in the corundum structure and has rhombohedral symmetry. The unit cell belongs to the $R\bar{3}c$ point group and contains 30 atoms [7]. The reduced primitive cell, used in this work, contains 10 atoms and is given in Figure 1.2. It is important to note, that the initial structure was derived from the experimental unit cell with hexagonal axes in [7] while calculations are performed with a primitive cell containing 10 atoms. This is possible within the trigonal crystal group where the rhombohedral lattice system can be described by hexagonal axes or rhombohedral axes. The experimental structure is equivalent to the corrundum structure and contains 30 atoms in the unit cell [7]. Note, that the used primitive cell in this work differs from the conventionally

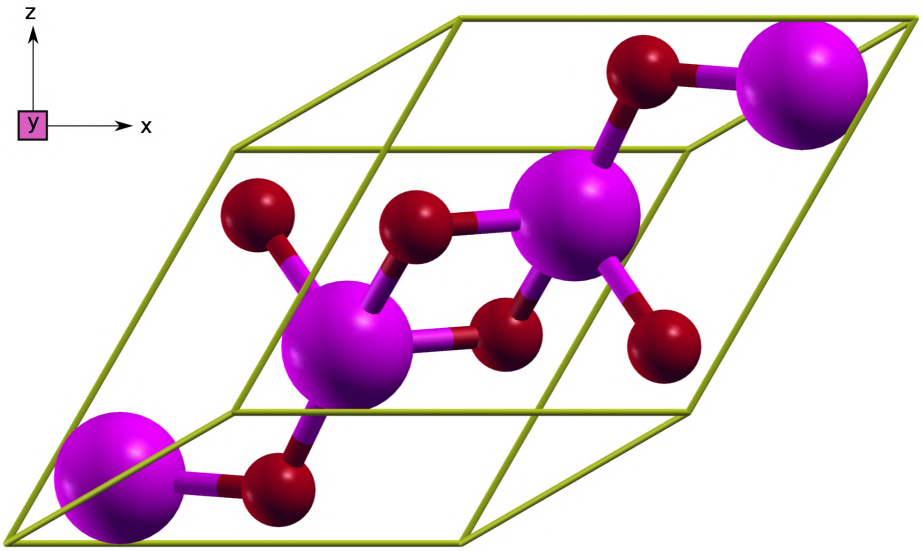

Figure 1.2: Schematic representation of the crystalline structure of the rhombohedral α phase of Ga_2O_3. Shown is the primitive cell with hexagonal axes containing 2 formula units. Gallium atoms are in purple and oxygen atoms in red.

used primitive cell with rhombohedral axes found in textbooks, such as [8].

The purpose of this work is to calculate the elastic properties of the α and β phase, especially the second-order elastic constants, from first principles. Although high pressure studies have been conducted, there are no results for the second-order elastic constants, as far as the author knows. Lattice parameters are investigated using the all-electron full-potential **`exciting`** code [9] and second-order elastic constants are calculated using the **`ElaStic@exciting`** tool [10].

2 Theoretical Foundations

In this chapter we give a brief introduction to the elasticity of a crystal. The focus is the derivation of the second-order elastic constants and computational methods which allow to calculate them. The theoretical approach to elasticity is given in Section 2.1, while Sections 2.2 and 2.3 will focus on the computational method of computing (elastic) properties of solids. They are based on total-energy calculations which can be performed using density-functional theory.

2.1 Introduction to elasticity

In this Section a short introduction of the theory of elasticity is given. A more in-depth discussion can be found in Refs. [11, 12, 13, 14].

Elasticity describes the reaction of materials to external forces and the resulting deformation of the structure. If these forces do not exceed a certain limit, the deformation vanishes with the removal of the forces. We call it *elastic deformation*. Nonvanishing *plastic deformations* will be neglected. Solids will be treated as homogeneous so that elastic properties can be derived from its unit cell as well as anisotropic so that elastic properties can be different in all directions. All theoretical derivations will be made in the elastic linear regime where the stress is proportional to the strain. Firstly, the concept of strain and stress is introduced.

2.1.1 Physical strain and stress

A simple illustration of the theory of elasticity is given by a spring. If it is stretched by an external force, a back-driving force $\boldsymbol{F}$ will appear that is proportional to the stretched distance. This is known as *Hooke's law*

$$\boldsymbol{F} = -k\,\boldsymbol{r}, \tag{2.1}$$

where boldface characters represent vectors and k the spring constant [15]. When the external and the back-driving force compensate each other, the spring will be in its new equilibrium configuration.

In order to find a generalized expression for Hooke's law, *stress* and *strain* will first be introduced through an intuitive picture.

Physical strain and stress

Consider a slab of an elastic material that is in its equilibrium state with no external forces acting on it. By applying a small strain that is stretching the slab perpendicular to its surface A while the bottom layer is fixed, the material will try to obtain a new equilibrium state where the external forces are compensated by internal forces acting on the nuclei on the surface. This situation is sketched in Figure 2.3.

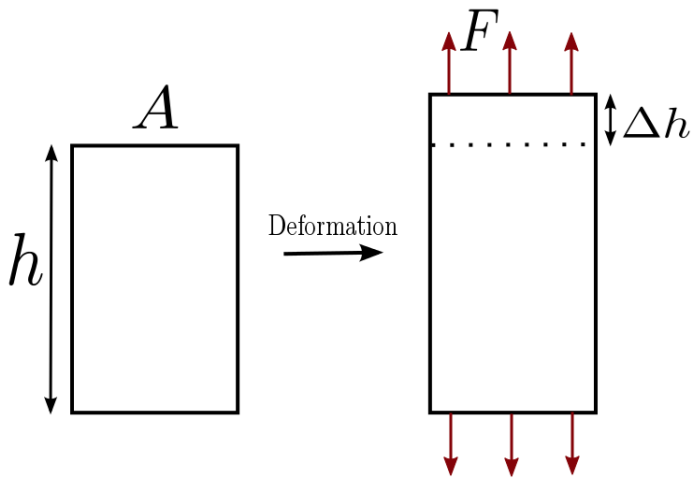

Figure 2.3: Schematic 2-dimensional representation of a deformation that varies the thickness. h represents the thickness, A the transverse area of the unit cell, F the sum of the external forces acting on the nuclei on the surface, and Δh the displacement.

In classical mechanics, an external work corresponds to a change in the energy. Since the material is in equilibrium in both states, only the potential energy U will undergo a change

$$\Delta U = \int_{h}^{h+\Delta h} F(z)\,\mathrm{d}z, \tag{2.2}$$

where F is the sum of the external forces acting on the nuclei of the top layer and Δh the ensuing displacement. Since the bottom layer is fixed, the work done by the external forces equals 0. The *physical stress* σ corresponds to the external force per unit area, $\sigma = F/A$. The *physical strain* ϵ is the displacement in relation to the original length, $\epsilon = \Delta h/h$. Inserting strain and stress into Eq. (2.2) yields:

$$\Delta U = V \int_{0}^{\epsilon} \sigma\,\mathrm{d}\epsilon, \tag{2.3}$$

with $V = Ah$. Remembering that we are in the linear regime and by introducing an elastic constant C, so that

$$\sigma = C\,\epsilon, \tag{2.4}$$

we obtain with Eq. (2.3):

$$\frac{\Delta U}{V} = \frac{1}{2} C\,\epsilon^2 \tag{2.5}$$

and finally:

$$\sigma = \frac{1}{V}\frac{\partial \Delta U}{\partial \epsilon}. \tag{2.6}$$

Equations (2.5) and (2.6) have been derived assuming that the stress and strain are along the same direction (see Figure 2.3), while this is not generally the case. In order to further generalize these equations, tensors have to be introduced. From now

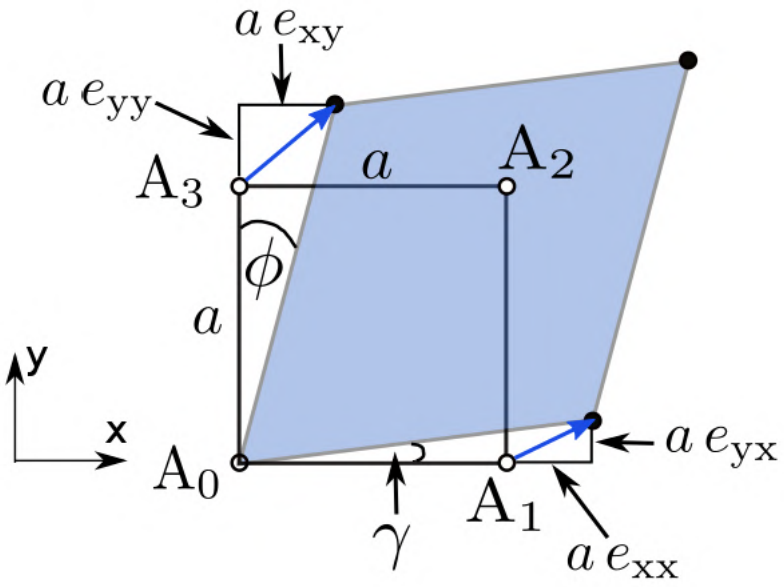

Figure 2.4: Schematic representation of an arbitrary 2 dimensional elastic deformation of a square lattice.

on, the *Einstein convention* will be used, where a summation is performed whenever two factors of a product have the same index.

In the general case of an arbitrary 2-dimensional deformation (see Figure 2.4) the change of coordinates for every material point can be written as [12]:

$$R'_\alpha = (\delta_{\alpha\beta} + e_{\alpha\beta})\, R_\beta, \tag{2.7}$$

where the indices α and β run over the Cartesian coordinates x, y, z, $\delta_{\alpha\beta}$ is Kronecker's delta, R'_α and R_β are the strained and unstrained nuclear positions, respectively, and $e_{\alpha\beta}$ is a 3×3 matrix with small elements $e_{\alpha\beta} \ll 1$. The coordinates of the material points A_1 and A_3 change according to Figure 2.4:

$$\begin{aligned} \boldsymbol{R}'_1 &= \boldsymbol{R}_1 + a\,(e_{xx}\hat{\boldsymbol{u}}_x + e_{yx}\hat{\boldsymbol{u}}_y) \\ \boldsymbol{R}'_3 &= \boldsymbol{R}_3 + a\,(e_{xy}\hat{\boldsymbol{u}}_x + e_{yy}\hat{\boldsymbol{u}}_y)\,, \end{aligned} \tag{2.8}$$

where $\hat{\boldsymbol{u}}_x$ and $\hat{\boldsymbol{u}}_y$ represent the unit vectors that span the x-y plane. It is important to note that these deformations implicitly include a rotation around the origin A_0. The A_0-A_1 connection is rotated counterclockwise by an angle γ around the origin while the A_0-A_3 connection is rotated clockwise by ϕ. Looking at Figure 2.4, γ and ϕ can be written as:

$$\tan\gamma = \frac{e_{yx}}{1 + e_{xx}} \tag{2.9}$$

$$\tan\phi = \frac{e_{xy}}{1 + e_{yy}} \tag{2.10}$$

Since only very small deformations and therefore also very small $e_{\alpha\beta}$ and angles are considered, it is valid to assume that $\tan\gamma \approx \gamma$, $\tan\alpha \approx \alpha$, and $(1 + e_{\alpha\beta}) \approx 1$, and

as such

$$\gamma \approx e_{yx}\,, \tag{2.11}$$

$$\alpha \approx e_{xy}\,. \tag{2.12}$$

Then the average counterclockwise rotation $(e_{yx} - e_{xy})/2$ has to be subtracted from the coordinate transformation in order to describe the deformation regardless of the rotation:

$$\boldsymbol{R}_1'' = \boldsymbol{R}_1' - \frac{a}{2}\left(e_{yx} - e_{xy}\right)\hat{\boldsymbol{u}}_y = \boldsymbol{R}_1 + a\left[e_{xx}\hat{\boldsymbol{u}}_x + \frac{1}{2}\left(e_{xy} + e_{yx}\right)\hat{\boldsymbol{u}}_y\right], \tag{2.13}$$

$$\boldsymbol{R}_3'' = \boldsymbol{R}_3' - \frac{a}{2}\left(e_{yx} - e_{xy}\right)\hat{\boldsymbol{u}}_x = \boldsymbol{R}_3 + a\left[e_{yy}\hat{\boldsymbol{u}}_y + \frac{1}{2}\left(e_{xy} + e_{yx}\right)\hat{\boldsymbol{u}}_x\right]. \tag{2.14}$$

It becomes evident that the pure elastic deformation is done by the symmetric part of $e_{\alpha\beta}$ while the antisymmetric part describes the rotation. This statement can be generalized [12]. The second-order *physical strain tensor* $\{\epsilon_{\alpha\beta}\}$, defined with elements

$$\epsilon_{\alpha\beta} = \frac{1}{2}\left(e_{\alpha\beta} + e_{\alpha\beta}\right), \tag{2.15}$$

ignores any rotations of the solid and is the generalization of the scalar physical strain introduced in Eq. (2.3). Any tensors from now on will be indicated by braces, *e.g.*, $\{\epsilon_{\alpha\beta}\}$. The general form of Eqs. (2.5) and (2.6) is [12]:

$$\frac{E}{V} = \frac{1}{2}\,C_{\alpha\beta\gamma\delta}\,\epsilon_{\alpha\beta}\,\epsilon_{\gamma\delta}\,, \tag{2.16}$$

and

$$\sigma_{\alpha\beta} = \frac{1}{V}\frac{\partial E}{\partial \epsilon_{\alpha\beta}}, \tag{2.17}$$

where E is the elastic energy, *e.g.*, the potential energy stored in the deformed state, $\{\sigma_{\alpha\beta}\}$ the second-order *physical stress tensor*, and $\{C_{\alpha\beta\gamma\delta}\}$ the fourth-order *stiffness tensor* consisting of $3^4 = 81$ elastic constants. The generalized Hooke's law is obtained by combining Eqs. (2.16) and (2.17) [11]:

$$\sigma_{\alpha\beta} = C_{\alpha\beta\gamma\delta}\,\epsilon_{\gamma\delta}. \tag{2.18}$$

The physical strain tensor $\{\epsilon_{\alpha\beta}\}$ is symmetric due to Eq. (2.15). Therefore the general form is

$$\{\epsilon_{\alpha\beta}\} = \begin{pmatrix} \epsilon_{xx} & \epsilon_{xy} & \epsilon_{xz} \\ \epsilon_{xy} & \epsilon_{yy} & \epsilon_{yz} \\ \epsilon_{xz} & \epsilon_{yz} & \epsilon_{zz} \end{pmatrix}. \tag{2.19}$$

The off-diagonal elements produce a *shear strain* while the diagonal elements correspond to a *normal strain*. A few 2-dimensional examples are given in Figure 2.5 where the physical strain tensors are:

$$(a) \quad \{\epsilon_{\alpha\beta}\} = \begin{pmatrix} \epsilon_{xx} & 0 \\ 0 & 0 \end{pmatrix}$$

$$(b) \quad \{\epsilon_{\alpha\beta}\} = \begin{pmatrix} \epsilon_{xx} & 0 \\ 0 & \epsilon_{yy} \end{pmatrix}$$

$$(c) \quad \{\epsilon_{\alpha\beta}\} = \begin{pmatrix} 0 & \epsilon_{xy} \\ \epsilon_{xy} & 0 \end{pmatrix}.$$

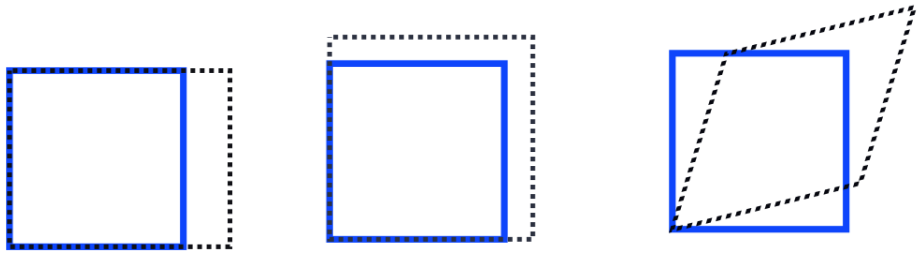

(a) Uniaxial strain (b) Expansion (c) Shear strain

Figure 2.5: Shown are three 2-dimensional deformations for different physical strain tensors. The blue squares, depicted with solid lines, represent the unstrained and the black dotted parallelograms the strained state, respectively.

Due to the fact that the physical strain tensor $\{\epsilon_{\alpha\beta}\}$ is symmetric and Eq. (2.17) is valid, it is evident that also the stress tensor $\{\sigma_{\alpha\beta}\}$ is symmetric and has the same form as Eq. (2.19).

As a way of simplifying symmetric tensors, it is common to use the *Voigt notation*, where the six independent components of the stress and strain tensors are rearranged in vectors with six components [13]:

$$\{\epsilon_{\alpha\beta}\} = \begin{pmatrix} \epsilon_{xx} & \epsilon_{xy} & \epsilon_{xz} \\ \epsilon_{xy} & \epsilon_{yy} & \epsilon_{yz} \\ \epsilon_{xz} & \epsilon_{yz} & \epsilon_{zz} \end{pmatrix} \rightarrow \boldsymbol{\epsilon} = \begin{pmatrix} \epsilon_1 \\ \epsilon_2 \\ \epsilon_3 \\ \epsilon_4 \\ \epsilon_5 \\ \epsilon_6 \end{pmatrix} \equiv \begin{pmatrix} \epsilon_{xx} \\ \epsilon_{yy} \\ \epsilon_{zz} \\ 2\epsilon_{yz} \\ 2\epsilon_{xz} \\ 2\epsilon_{xy} \end{pmatrix} \tag{2.20}$$

$$\{\sigma_{\alpha\beta}\} = \begin{pmatrix} \sigma_{xx} & \sigma_{xy} & \sigma_{xz} \\ \sigma_{xy} & \sigma_{yy} & \sigma_{yz} \\ \sigma_{xz} & \sigma_{yz} & \sigma_{zz} \end{pmatrix} \rightarrow \boldsymbol{\sigma} = \begin{pmatrix} \sigma_1 \\ \sigma_2 \\ \sigma_3 \\ \sigma_4 \\ \sigma_5 \\ \sigma_6 \end{pmatrix} \equiv \begin{pmatrix} \sigma_{xx} \\ \sigma_{yy} \\ \sigma_{zz} \\ \sigma_{yz} \\ \sigma_{xz} \\ \sigma_{xy} \end{pmatrix} \tag{2.21}$$

By introducing the factor 2 in the shear strain components, the scalar invariance $\sigma_{\alpha\beta}\,\epsilon_{\alpha\beta} = \boldsymbol{\sigma} \cdot \boldsymbol{\epsilon}$ is preserved.

Also the stiffness tensor can be written in Voigt notation. Considering that $\sigma_{\alpha\beta} = \sigma_{\beta\alpha}$ and $\epsilon_{\gamma\delta} = \epsilon_{\delta\gamma}$, and the fact that Eq. (2.18) is invariant with respect to the change of the pairs of indices $\alpha\beta$ and $\gamma\delta$, the stiffness tensor has 21 independent components. It can be therefore written as a symmetric 6×6 matrix [13]:

$$\{C_{\alpha\beta\gamma\delta}\} \rightarrow \boldsymbol{C} = \begin{pmatrix} C_{11} & C_{12} & C_{13} & C_{14} & C_{15} & C_{16} \\ C_{12} & C_{22} & C_{23} & C_{24} & C_{25} & C_{26} \\ C_{13} & C_{23} & C_{33} & C_{34} & C_{35} & C_{36} \\ C_{14} & C_{24} & C_{34} & C_{44} & C_{45} & C_{46} \\ C_{15} & C_{25} & C_{35} & C_{45} & C_{55} & C_{56} \\ C_{16} & C_{26} & C_{36} & C_{46} & C_{56} & C_{66} \end{pmatrix}. \tag{2.22}$$

The generalized Hooke's law can then be written as

$$\boldsymbol{\sigma} = \boldsymbol{C} \cdot \boldsymbol{\epsilon}, \tag{2.23}$$

while Eq. (2.16) can be restated as:

$$\frac{E}{V} = \frac{1}{2}\, \boldsymbol{\epsilon}^{\intercal} \cdot \boldsymbol{C} \cdot \boldsymbol{\epsilon}, \tag{2.24}$$

where $\boldsymbol{\epsilon}^{\intercal}$ is the transpose of $\boldsymbol{\epsilon}$. Equation (2.23) can be inverted to the form

$$\boldsymbol{\epsilon} = \boldsymbol{S} \cdot \boldsymbol{\sigma}\,, \tag{2.25}$$

where $\boldsymbol{S} = \boldsymbol{C}^{-1}$ is the second-rank *compliance tensor* [13]. The deformation tensor $\boldsymbol{T}$ that describes the change of position $\boldsymbol{R}_\alpha$ of the material point α without global rotation

$$\boldsymbol{R}'_\alpha = \boldsymbol{T}\, \boldsymbol{R}_\alpha, \tag{2.26}$$

has the form

$$\boldsymbol{T} = 1 + \boldsymbol{\epsilon}. \tag{2.27}$$

In principle, the elastic constants can be calculated using only Eq. (2.24) and by calculating the elastic energy.

2.1.2 Example: Elastic constants of a rhombohedral crystal

The calculation of the elastic constants of a rhombohedral crystal, *e.g.*, the α phase of Ga_2O_3, will be outlined in this section as an example of calculations in the framework of the theory of elasticity.

In this case, the stiffness tensor has 6 independent components due to the symmetry of the crystal and has the following form in the Voigt notation [13]:

$$\boldsymbol{C} = \begin{pmatrix} C_{11} & C_{12} & C_{13} & C_{14} & 0 & 0 \\ C_{12} & C_{11} & C_{13} & -C_{14} & 0 & 0 \\ C_{13} & C_{13} & C_{33} & 0 & 0 & 0 \\ C_{14} & -C_{14} & 0 & C_{44} & 0 & 0 \\ 0 & 0 & 0 & 0 & C_{44} & C_{14} \\ 0 & 0 & 0 & 0 & C_{14} & \frac{1}{2}\,(C_{11} - C_{12}) \end{pmatrix}. \tag{2.28}$$

Evaluating the elastic energy per volume in Eq. (2.24) gives the following result:

$$\begin{aligned} \frac{E}{V} = \frac{1}{2}\Big[C_{11}\left(\epsilon_1^2 + \epsilon_2^2 + \frac{1}{2}\epsilon_6^2\right) + C_{12}\left(2\,\epsilon_1\,\epsilon_2 - \frac{1}{2}\,\epsilon_6^2\right) + 2\,C_{13}\,(\epsilon_1\,\epsilon_3 + \epsilon_2\,\epsilon_3) + \\ C_{14}\,(\epsilon_1\,\epsilon_4 + 2\,\epsilon_5\,\epsilon_6) + C_{33}\,\epsilon_3^2 + C_{44}\left(\epsilon_4^2 + \epsilon_5^2\right)\Big]. \end{aligned} \tag{2.29}$$

Three different deformations have to be applied in order to determine three different elastic constants although the choice of these deformations is not distinct.

A possible choice consists of a uniaxial deformation of the unit cell by a parameter ε. Equation (2.30) then takes on the form:

$$\boldsymbol{\epsilon}_1 = \begin{pmatrix} 0 \\ 0 \\ \varepsilon \\ 0 \\ 0 \\ 0 \end{pmatrix} \rightarrow \frac{E}{V} = \frac{1}{2} C_{33}\, \varepsilon^2. \tag{2.30}$$

The second type could be another uniaxial deformation in the form of:

$$\boldsymbol{\epsilon}_2 = \begin{pmatrix} \varepsilon \\ 0 \\ 0 \\ 0 \\ 0 \\ 0 \end{pmatrix} \rightarrow \frac{E}{V} = \frac{1}{2} C_{11}\, \varepsilon^2. \tag{2.31}$$

For the third one, a shear deformation could be considered:

$$\boldsymbol{\epsilon}_3 = \begin{pmatrix} 0 \\ 0 \\ 0 \\ \varepsilon \\ 0 \\ 0 \end{pmatrix} \rightarrow \frac{E}{V} = \frac{1}{2} C_{44}\, \varepsilon^2. \tag{2.32}$$

The fourth one could be another shear deformation:

$$\boldsymbol{\epsilon}_4 = \begin{pmatrix} 0 \\ 0 \\ 0 \\ 0 \\ 0 \\ \varepsilon \end{pmatrix} \rightarrow \frac{E}{V} = \frac{1}{4} \left(C_{11} - C_{12}\right) \varepsilon^2. \tag{2.33}$$

For the fifth type, a biaxial deformation could be considered:

$$\boldsymbol{\epsilon}_5 = \begin{pmatrix} \varepsilon \\ 0 \\ \varepsilon \\ 0 \\ 0 \\ 0 \end{pmatrix} \rightarrow \frac{E}{V} = \frac{1}{2} \left(C_{11} + C_{33} + 2C_{13}\right) \varepsilon^2. \tag{2.34}$$

The final one could be the combination of a shear and uniaxial deformation:

$$\boldsymbol{\epsilon}_5 = \begin{pmatrix} \varepsilon \\ 0 \\ 0 \\ \varepsilon \\ 0 \\ 0 \end{pmatrix} \rightarrow \frac{E}{V} = \frac{1}{2} \left(C_{14} + C_{11} + C_{44}\right) \varepsilon^2. \tag{2.35}$$

The 6 elastic constants for a rhombohedral crystal can then be computed by calculating the elastic energies for all three deformation types and solving the resulting system of linear equations.

2.1.3 Langrangian strain and stress

Within the theory of elasticity, different kinds of strain and stress can be definded. A possible choice is the *Lagrangian strain and stress*. Instead of measuring the positions of material points in the strained and unstrained position, it is also legitimate to measure the change of distance between 2 material points [13]

$$|\Delta \boldsymbol{R}'|^2 - |\Delta \boldsymbol{R}|^2 = 2\,\eta_{\alpha\beta}\,\Delta R_\alpha\,\Delta R_\beta, \tag{2.36}$$

where $|\Delta \boldsymbol{R}|$ and $|\Delta \boldsymbol{R}'|$ represent the distance between 2 material points in the unstrained and strained configuration, respectively, and $\{\eta_{\alpha\beta}\}$ is the *Lagrangian strain tensor* [13]:

$$\eta_{\alpha\beta} = \epsilon_{\alpha\beta} + \frac{1}{2}\,\epsilon_{\gamma\alpha}\,\epsilon_{\gamma\beta}. \tag{2.37}$$

The components of the *Lagrangian stress tensor* $\{\tau_{\alpha\beta}\}$ are defined as [13]:

$$\tau_{\alpha\beta} = \det(1+\epsilon_{\alpha\beta})(1+\epsilon_{\alpha\gamma})^{-1}\,\sigma_{\gamma\delta}\,(1+\epsilon_{\delta\beta})^{-1}. \tag{2.38}$$

It is evident that $\{\eta_{\alpha\beta}\}$ and $\{\tau_{\alpha\beta}\}$ are symmetric second-rank tensors. Therefore the Lagrangian strain and stress can also be written in the Voigt notation, *e.g.*, $\{\eta_{\alpha\beta}\} \equiv \boldsymbol{\eta}$ and $\{\tau_{\alpha\beta}\} \equiv \boldsymbol{\tau}$.

2.1.4 Alternative method of deriving elastic constants

When considering only small strains, it is also possible to express the total energy per volume of a crystal as a Taylor expansion in terms of the strain, *e.g.*, $\boldsymbol{\eta}$, around the equlibrium [13]:

$$\frac{E(\boldsymbol{\eta})}{V_0} = \frac{E_0}{V_0} + \underbrace{(\boldsymbol{\tau}_0 \cdot \eta)}_{=\,0} + \left(\frac{1}{2!}\,\boldsymbol{\eta}^\intercal \cdot \boldsymbol{C} \cdot \boldsymbol{\eta}\right) + \ldots, \tag{2.39}$$

where E_0 and V_0 refer to the equilibrium energy and volume, and

$$\boldsymbol{\tau}_0 = \frac{1}{V_0}\,\frac{\partial E}{\partial\,\boldsymbol{\eta}}\bigg|_{\boldsymbol{\eta}=0}, \tag{2.40}$$

to the stress in equilibrium. The first term vanishes because there are no forces acting on the solid at equilibrium and therefore also no stress is present. In the second term, $\boldsymbol{C}$ represents the stiffness tensor and it can be derived by two equivalent equations, according to Eq. (2.39) or (2.23)

$$\boldsymbol{C} = \frac{1}{V_0}\,\frac{\partial^2 E}{\partial\,\boldsymbol{\eta}\,\partial\,\boldsymbol{\eta}}\bigg|_{\boldsymbol{\eta}=0} \tag{2.41}$$

and

$$\boldsymbol{C} = \frac{\partial\,\boldsymbol{\tau}}{\partial\,\boldsymbol{\eta}}\bigg|_{\boldsymbol{\eta}=0}. \tag{2.42}$$

As a result, the second-order elastic constants can also be derived by numerically calculating these derivatives at the reference configuration. This procedure is implemented in the `ElaStic` tool [10].

The independent components of the stiffness tensor can be calculated by applying a set of properly chosen deformation types and solving the system of linear equations, similar to the procedure described in the previous section. Using this approach, it is also possible to derive higher-order elastic constants by considering more terms in the expansion in Eq. (2.39). In the previous chapters only the stiffness tensor was introduced, as a result of considering the linear elastic regime. The existence of higher-order elastic constants can then be interpreted as nonlinear effects which describe the deviation from the linear regime.

It is important to note that only the second-order elastic constants are the same for the physical and Langrangian strain, due to Eq. (2.37). Therefore it is important to specify what type of strain is used for the expansion when calculating higher-order elastic constants.

2.1.5 Elastic moduli

There are several *elastic moduli* that represent linear combinations of elastic constants. An example are the isotropic elastic moduli such as the bulk modulus B, the shear modulus G, the Young modulus E and the Poisson ratio ν. In the Voigt approach a uniform strain is assumed [16], while in the Reuss approach a uniform stress is assumed [17], denoted by the subscript V and R, respectively. Therefore, the definitions for the moduli differ [16, 17]

$$B_{\mathrm{V}} = \frac{1}{9}\left[(C_{11}+C_{22}+C_{33})+2(C_{12}+C_{13}+C_{23})\right], \tag{2.43}$$

$$G_{\mathrm{V}} = \frac{1}{15}\left[(C_{11}+C_{22}+C_{33})-(C_{12}+C_{13}+C_{23})+3(C_{44}+C_{55}+C_{66})\right], \tag{2.44}$$

and

$$B_{\mathrm{R}} = \left[(S_{11}+S_{22}+S_{33})+2\left(S_{12}+S_{13}+S_{23}\right)\right]^{-1}, \tag{2.45}$$

$$G_{\mathrm{R}} = 15\left[4\left(S_{11}+S_{22}+S_{33}\right)-\left(S_{12}+S_{13}+S_{23}\right)+3\left(S_{44}+S_{55}+S_{66}\right)\right]^{-1}, \tag{2.46}$$

where $S_{\alpha\beta}$ are the components of the compliance tensor $\boldsymbol{S}$. Hill has shown that the Voigt and Reuss elastic moduli are the strict upper and lower bound, respectively [18, 19]. As a result, the Hill averaged elastic moduli, denoted by the subscript H, are

$$B_{\mathrm{H}} = \frac{1}{2}\left(B_{\mathrm{V}}+B_{\mathrm{R}}\right), \tag{2.47}$$

$$G_{\mathrm{H}} = \frac{1}{2}\left(G_{\mathrm{V}}+G_{\mathrm{R}}\right). \tag{2.48}$$

The Young modulus, E, and Poisson ratio, ν, can defined in dependence on the bulk, B, and shear modulus, G, for all the three approaches, according to:

$$E = \frac{9BG}{3B+G}, \tag{2.49}$$

$$\nu = \frac{3B-2G}{2\left(3B+G\right)}. \tag{2.50}$$

2.2 Atomistic view of the elastic energy

The main task of determining second-order elastic constants is the calculation of the total elastic energy in Eq. 2.24. In the theory of elasticity introduced in the previous section, the elastic energy was defined for a continuous material consisting of material points. A solid, however, is made up of atoms which consist of nuclei and electrons. Therefore it is necessary to define the elastic energy in this context. This section will introduce energy calculations using density-functional theory and its implementation in the **exciting** code.

If one wants to calculate the electronic structure of materials, it is necessary to solve the many-body Schrödinger equation (spin dependency is here not explicitly written)

$$\hat{H}\,\Psi\left(\widetilde{r},\widetilde{R}\right)=\mathcal{E}\,\Psi\left(\widetilde{r},\widetilde{R}\right), \tag{2.51}$$

where $\hat{H}$ represents the total many-body Hamiltonian dependent on both the electron $\widetilde{r}=\{\mathbf{r}_i, i=1,\ldots,N\}$[1] and nuclei positions $\widetilde{R}=\{\mathbf{R}_I, I=1,\ldots,N_\mathrm{n}\}$, N the number of electrons, N_n the number of nuclei, $\mathcal{E}$ the energy eigenvalue of the coupled system consisting of nuclei and electrons and Ψ the total many-body wavefunction. As a result this equation has $3N+3N_\mathrm{n}$ independent variables. By using the *Born-Oppenheimer approximation*, the nuclei can be viewed as nearly stationary due to the high mass and slow velocity compared to the electrons [20]. Therefore the total wavefunction can be separated by using the ansatz:

$$\Psi\left(\widetilde{r},\widetilde{R}\right)=\sum_a \chi_a(\widetilde{R})\cdot\Phi_a^\mathrm{el}(\widetilde{r};\widetilde{R}). \tag{2.52}$$

The semicolon in the electronic wavefunction Φ^el is there to show that it is still dependent on the nuclei coordinates although they can be viewed as parameters.

This approximation reduces the problem to $3N$ variables in the form

$$\hat{H}^\mathrm{el}\,\Phi^\mathrm{el}\left(\widetilde{r};\widetilde{R}\right)=E^\mathrm{el}\left(\widetilde{R}\right)\,\Phi^\mathrm{el}\left(\widetilde{r};\widetilde{R}\right). \tag{2.53}$$

The energy eigenvalue $E^\mathrm{el}\left(\widetilde{R}\right)$ of the electronic many-body system corresponds to the elastic energy that has to be calculated. The electronic Hamiltonian has the following components

$$\hat{H}^\mathrm{el}=\hat{T}+\hat{U}+\hat{V}+V_\mathrm{n-n}(\widetilde{R}), \tag{2.54}$$

with

$$\begin{aligned}
\hat{T}&=\sum_{i=1}^{N}\left(\frac{-\nabla_i^2}{2}\right),\\
\hat{U}&=\frac{1}{2}\sum_{i=1}^{N}\sum_{\substack{j=1\\ i\neq j}}^{N}\frac{1}{|\mathbf{r}_i-\mathbf{r}_j|},\\
\hat{V}&=\frac{1}{2}\sum_{i=1}^{N}\sum_{I=1}^{N_\mathrm{n}}\frac{Z_\mathrm{n}}{|\mathbf{r}_i-\mathbf{R}_I|}=:\sum_{i}^{N}v(\mathbf{r}_i),
\end{aligned}$$

[1] Note that $\widetilde{r}$ refers to the collectivity of all electron positions while $\mathbf{r}$ represents the postion vector of a single electron, described by 3 coordinates.

where $\hat{T}$ is the kinetic-energy operator, $\hat{U}$ the repulsive Coulomb-interaction operator between the electrons, $\hat{V}$ the attractive Coulomb-interaction operator between nuclei and electrons, and $V_{\mathrm{n-n}}(\widetilde{R})$ a constant contribution (at a given $\widetilde{R}$) due to the Coulomb interaction between the nuclei. From now on will this constant $V_{\mathrm{n-n}}(\widetilde{R})$ be included in the external potential operator $\hat{V}$. This is still a many-body problem with $3N$ independent variables. In order to further lower the computational cost, additional methods have to be considered, such as density-functional theory.

2.2.1 Density-Functional Theory

The *density-functional theory* (*DFT*) is a method to calculate the ground-state properties of atoms, moleculs and solids. The starting point is given by the *Hohenberg-Kohn theorem*, which consists of two parts [21]. Part one states that there is a one-to-one correspondence between the ground-state electron density $n_{\mathrm{GS}}(\mathbf{r})$ and the external potential $v(\mathbf{r})$. Due to the fact that the external potential defines the Hamiltonian and as such the system, any observable can be written as a functional of n_{GS}. Therefore the total ground-state energy E_{GS} is a unique functional of the ground-state electron density $n_{\mathrm{GS}}(\mathbf{r})$:

$$E_{\mathrm{GS}}[n_{\mathrm{GS}}] = F[n_{\mathrm{GS}}] + \int v(\mathbf{r})\, n_{\mathrm{GS}}(\mathbf{r})\, \mathrm{d}\mathbf{r}. \tag{2.55}$$

The second part states that the total ground-state energy takes its minimum at the ground-state density. This means that the task is to minimize the total energy functional in Eq. (2.55) with respect to n under the condition

$$\int n(\mathbf{r})\, \mathrm{d}\mathbf{r} = N. \tag{2.56}$$

To take this restriction into account, the method of Lagrange multipliers is used. An auxiliary functional

$$A(\mu, [n]) = E_{\mathrm{GS}}[n] - \mu \left(\int n(\mathbf{r})\, \mathrm{d}\mathbf{r} - N \right) \tag{2.57}$$

is introduced that has to be minimized with respect to n:

$$\left. \frac{\delta A(\mu, [n])}{\delta n} \right|_{n=n_{\mathrm{GS}}} \stackrel{!}{=} 0. \tag{2.58}$$

The energy functional $F[n]$ is the same for every system and can be written as:

$$F[n] = T[n] + U[n] = T_0[n] + E_{\mathrm{H}}[n] + E_{\mathrm{XC}}[n]. \tag{2.59}$$

The contribution $T_0[n]$ represents the kinetic-energy functional of N non-interacting electrons with an electron density $n(\mathbf{r})$, $E_{\mathrm{H}}[n]$ is the Hartree energy functional and $E_{\mathrm{XC}}[n]$ the exchange-correlation energy functional. This is still an exact expression. Solving Eq. 2.58, by taking Eqs. (2.55) and (2.59) into account, yields the following result:

$$\left(\frac{\delta T_0[n]}{\delta n(\mathbf{r})} + v_{\mathrm{KS}}(\mathbf{r}; [n]) \right) \Bigg|_{n=n_{\mathrm{GS}}} = \mu, \tag{2.60}$$

with

$$v_{\mathrm{KS}}(\mathbf{r};[n]) = \frac{\delta E_{\mathrm{H}}(\mathbf{r},[n])}{\delta n(\mathbf{r})} + \frac{\delta E_{\mathrm{XC}}(\mathbf{r},[n])}{\delta n(\mathbf{r})} + v(\mathbf{r}) \tag{2.61}$$

$$\stackrel{!}{=} v_{\mathrm{H}}(\mathbf{r};[n]) + v_{\mathrm{XC}}(\mathbf{r};[n]) + v(\mathbf{r}). \tag{2.62}$$

Equation (2.60) resembles the problem for a system consisting of N non-interacting electrons in an effective external potential v_{KS}. Due to this mathematical equivalence, the equation can be solved in the same way:[2]

$$\left(-\frac{\nabla^2}{2} + v_{\mathrm{KS}}(\mathbf{r};[n])\right)\varphi_\gamma(\mathbf{r}) = \varepsilon_\gamma\,\varphi_\gamma(\mathbf{r}), \tag{2.63}$$

with

$$n(\mathbf{r}) = \sum_{\gamma}^{\mathrm{occ}} \left|\varphi_\gamma(\mathbf{r})\right|^2, \tag{2.64}$$

where $\sum_{\gamma}^{\mathrm{occ}}$ represents the summation over all occupied states. Equations (2.63) and (2.64) are known as the *Kohn-Sham equations*, where $\{\varphi_\gamma(\mathbf{r})\}$ represent the Kohn-Sham wavefunctions [22]. It is important to point out that $\varphi_\gamma(\mathbf{r})$ and ε_γ have no physical meaning. They cannot be used to describe the real system of interacting electrons although the calculated ground-state electron density is the exact one. The Kohn-Sham equations have to be solved self-consistently according to the scheme in Figure (2.6). Up to this point no approximation has been made. A problem arises by examining the exchange correlation potential $v_{\mathrm{XC}}[n]$. The exact expression is to this day unknown. As a result, the accuracy of the DFT calculation depends on the level of approximation for $v_{\mathrm{XC}}[n]$. Many approximations for the exchange correlation functional with varying accuracy have been proposed in the literature, among the most used are the local-density approximation (LDA) [23] and the generalized gradient approximation (GGA), *e.g.*, the PBE [24] and the PBEsol functional [25].

2.2.2 Numerical solutions of the Kohn-Sham equations

In order to find $\varphi_\gamma(\mathbf{r})$ one has to solve the KS equations numerically. For an actual computational implementation, it is necessary to describe these wavefunctions in terms of a known *basis set*

$$\varphi_\gamma(\mathbf{r}) = \sum_{p=1}^{P} c_\gamma^p\,\phi_\gamma^p(\mathbf{r}), \tag{2.65}$$

that properly describes physical properties as well as keeps the computational cost manageable. Only a limited amount of basis functions can be considered. Therefore, it is important to choose a basis set that requires few basis functions but still provides sufficient accuracy. Given a fixed P, inserting Eq. (2.65) in Eq. (2.63) yields an eigenvalue problem:[3]

$$(H - \varepsilon\, O)\,\mathcal{C} = 0. \tag{2.66}$$

[2]Note that the energy eigenvalue ε_γ is not to be confused with the strain ϵ.

[3]The explicit dependence on γ is omitted.

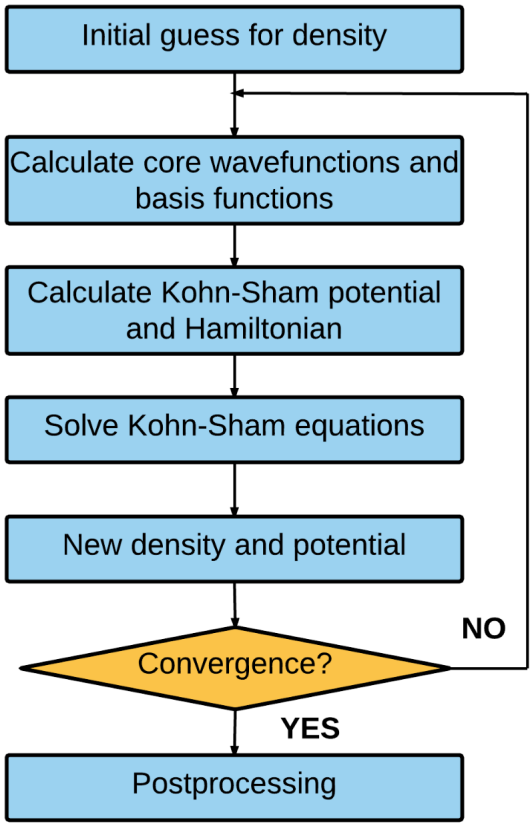

Figure 2.6: Flowchart for the self consistent solution of the Kohn-Sham equations using an unspecified basis set.

H is defined as the Hamiltonian matrix with the elements

$$H_{il} = \left\langle \phi_\gamma^i \middle| -\frac{\nabla^2}{2} + v_{\mathrm{KS}} \middle| \phi_\gamma^l \right\rangle \tag{2.67}$$

and the overlap matrix O has the elements

$$O_{il} = \left\langle \phi_\gamma^i \middle| \phi_\gamma^l \right\rangle . \tag{2.68}$$

The eigenvector $\mathcal{C}$ consists of the coefficients c_γ^p given in Eq. (2.65) and $\varepsilon = \varepsilon_\gamma$ contains the energy eigenvalues. The computation time depends on the process of diagonalizing the matrix in Eq. (2.67) and therefore on the number of basis functions P.

A simple basis set is given by plane waves:

$$\varphi_{\mathrm{n}\boldsymbol{k}}(\mathbf{r}) = \frac{1}{\sqrt{\Omega}} \sum_{|\boldsymbol{k}+\boldsymbol{G}| \leq G_{\max}} c_{n\boldsymbol{k}}^{\boldsymbol{k}+\boldsymbol{G}} \mathrm{e}^{\mathrm{i}(\boldsymbol{k}+\boldsymbol{G})\cdot\mathbf{r}}, \tag{2.69}$$

where $\boldsymbol{G}$ corresponds to the reciprocal lattice vector and Ω to the volume of the crystal. Due to the fact that plane waves are orthogonal, the overlap matrix in Eq. 2.68 is a unit matrix and Eq. 2.66 becomes a linearized eigenvalue problem. Near the nuclei, the electronic wavefunction shows a highly oscillating behavior and therefore a very high number of plane waves is required to describe this region. This would result in very high $G_{\max}$ values and the large size of the matrices in Eq. (2.67) would make the computational time very high.

2.3 (L)APW + lo Method

This section will introduce the (L)APW + lo basis set, implemented in the **exciting** code, used for all calculations in the present work.

Electrons far away from the nuclei act as almost "free" electrons and can accurately be described by plane waves. Near the nuclei the electronic wavefunction resembles more atomic like wavefunctions. As a result, one can separate the space into two regions, the interstitial region (I) and the muffin-tin region (MT). These MTs are spheres with a radius of R_{MT} centered on the atoms labeled by $\mathbf{R}_\alpha$.[4] The KS wavefunctions can be written as [26]

$$\varphi_{n\boldsymbol{k}}(\mathbf{r}) = \sum_{\boldsymbol{G}} c^{\boldsymbol{k}}_{n\boldsymbol{G}}\, \phi_{\boldsymbol{k}+\boldsymbol{G}}(\mathbf{r}), \tag{2.70}$$

where

$$\phi_{\boldsymbol{k}+\boldsymbol{G}}(\boldsymbol{r}) = \begin{cases} \sum\limits_{lm} A^{\boldsymbol{k}+\boldsymbol{G}}_{lm\alpha}\, u_{l\alpha}(r_\alpha, \varepsilon_{nk})\, Y_{lm}(\hat{\mathbf{r}}_\alpha), & r_\alpha \leq R_{\mathrm{MT}} \\ \frac{1}{\sqrt{\Omega}} \mathrm{e}^{\mathrm{i}(\boldsymbol{k}+\boldsymbol{G})\cdot\mathbf{r}}, & \mathbf{r} \in I \end{cases} \tag{2.71}$$

where $\mathbf{r}_\alpha = \mathbf{r} - \mathbf{R}_\alpha$. The muffin-tin region is expanded in terms of spherical harmonics $Y_{lm}(\hat{\mathbf{r}}_\alpha)$ and radial functions $u_{l\alpha}(r_\alpha, \varepsilon_{nk})$, whereas $A^{\boldsymbol{k}+\boldsymbol{G}}_{lm\alpha}$ are the coefficients that are obtained by the continuity condition at the sphere boundary. In order to linearize the eigenvalue problem, the radial function $u_{l\alpha}(r_\alpha, \varepsilon_{nk})$ is expanded around the linearization energy in a Taylor expansion up to the first-order:

$$u_{l\alpha}(r_\alpha, \varepsilon_{nk}) \approx u_{l\alpha}(r_\alpha, \varepsilon_{l\alpha}) + (\varepsilon_{l\alpha} - \varepsilon_{nk}) \underbrace{\left.\frac{\partial u_{l\alpha}(r_\alpha, \varepsilon)}{\partial \varepsilon}\right|_{\varepsilon=\varepsilon_{l\alpha}}}_{\dot{u}_{l\alpha}(r_\alpha, \varepsilon_{l\alpha})}. \tag{2.72}$$

Plugging this equation into Eq. (2.71) gives the definition of the *linearized augmented planewaves* (LAPW) basis set [26]

$$\phi_{\boldsymbol{k}+\boldsymbol{G}}(\mathbf{r}) = \begin{cases} \sum\limits_{lm} \left[A^{\boldsymbol{k}+\boldsymbol{G}}_{lm\alpha}\, u_{l\alpha}(r_\alpha, \varepsilon_{l\alpha}) + B^{\boldsymbol{k}+\boldsymbol{G}}_{lm\alpha}\, \dot{u}_{l\alpha}(r_\alpha, \varepsilon_{l\alpha}) \right] Y_{lm}(\hat{\mathbf{r}}_\alpha), & r_\alpha \leq R_{\mathrm{MT}} \\ \frac{1}{\sqrt{\Omega}}\, \mathrm{e}^{\mathrm{i}(\boldsymbol{k}+\boldsymbol{G})\cdot\mathbf{r}}, & \mathbf{r} \in I. \end{cases} \tag{2.73}$$

The coefficient $B^{\boldsymbol{k}+\boldsymbol{G}}_{lm\alpha}$ has to be introduced because the energy difference $(\varepsilon_{l\alpha} - \varepsilon_{nk})$ is an unknown quantity. The way to determine both $A^{\boldsymbol{k}+\boldsymbol{G}}_{lm\alpha}$ and $B^{\boldsymbol{k}+\boldsymbol{G}}_{lm\alpha}$, is the continuity condition of $\phi_{\boldsymbol{k}+\boldsymbol{G}}(\mathbf{r})$ as well as its spatial derivative at the muffin-tin boundary. However, this approach harbors additional problems such as the disability to describe states with the same l but different principal quantum numbers. This applies to cases where the elements have valence as well as core electrons.

An alternative approach to the linearization of the radial functions is given by the introduction of *local orbitals* (lo) [27]. These local orbitals

$$\phi_\beta(\mathbf{r}) = \begin{cases} \delta_{\alpha\alpha_\beta}\delta_{ll_\beta}\delta_{mm_\beta} \left[a_\beta u_{l\alpha}(r_\alpha, \varepsilon_{l\alpha}) + b_\beta \dot{u}_{l\alpha}(r_\alpha, \varepsilon_{l\alpha}) \right] Y_{lm}(\hat{\mathbf{r}}_\alpha), & r_\alpha \leq R_{\mathrm{MT}} \\ 0, & \mathbf{r} \in I \end{cases} \tag{2.74}$$

[4] The muffin-tin radii R_{MT} can vary for different atoms.

are added to the LAPW basis functions with fixed energy parameters, where the parameters a_β and b_β are forcing $\phi_\beta = 0$ at the muffin-tin boundary and $\int_\Omega |\phi_\beta(\mathbf{r})|^2 \, \mathrm{d}^3\mathrm{r} = 1$. The wavefunction with the (L)APW+lo basis set takes on the form

$$\varphi_{nk}(\mathbf{r}) = \sum_{\boldsymbol{G}} c^{\boldsymbol{k}}_{n\boldsymbol{G}} \, \phi_{\boldsymbol{k}+\boldsymbol{G}}(\mathbf{r}) + \sum_{\beta} c^{\boldsymbol{k}}_{n\beta} \, \phi_\beta(\mathbf{r}). \tag{2.75}$$

Compared to the LAPW basis set, this introduction of local orbitals results in a smaller linearization error while the error in total energy is still $\mathcal{O}(\epsilon_{l\alpha} - \varepsilon_{nk})^4$ [9].

The basis is now completely defined and can be used to solve Eq. (2.67). The dimension of the matrices H and O are limited by the condition $|\boldsymbol{k} + \boldsymbol{G}| \leq G_{\max}$. This plane wave cutoff $G_{\max}$ alone is not an appropriate parameter if the muffin-tin radius R_{MT} is reduced, because then more plane waves are required to accurately describe the interstitial region. This is due to the fact that this region now contains parts where the wavefunction is varying stronger. In other words, a decrease of R_{MT} requires an increase of $G_{\max}$ in order to achieve the same level of accuracy. Therefore a more appropriate dimensionless cutoff parameter is the product $R^{\min}_{\mathrm{MT}} G_{\max}$, where $R^{\min}_{\mathrm{MT}}$ corresponds to the smallest muffin-tin radius.

2.3.1 Implementation of (L)APW+lo basis set in `exciting`

The basis sets used for calculations are defined by species files within the **`exciting`** code [9]. In Appendix A, the used species files for gallium and oxygen can be found with the chosen energy parameters. They will be used for all following calculations. For a detailed description of the structure of the species file, see [9] and the **`exciting`** web site.[5]

2.4 The `ElaStic` tool

Combining the theory of elasticity, presented in Section 2.1, with the calculation of the elastic energy by using DFT in the **`exciting`** code, outlined in Sections 2.2 and 2.3, enables the calculation of second-order elastic constants. The procedure depicted in Figure 2.7 is implemented in the **`ElaStic@exciting`** code [10].

The energy expansion in Eq. (2.39) is done in terms of the Lagrangian strain $\boldsymbol{\eta}$. Therefore, the second-order elastic constants are also derived with the Lagrangian strain. While second-order elastic constants are equal for physical and Lagrangian strain, higher-order elastic constants differ for both definitions. The derivation of higher-order elastic constants in the literature is usually done in terms of the Lagrangian strain, *e.g.*, in [13]. In this work only the second-order elastic constants are calculated.

Since the second-order elastic constants are calculated as a derivative of the energy, see Eq. (2.41) they are subjected to uncertainties in the energy calculations. These can be the result of many factors, *e.g.*, an insufficient amount of strain points used in the energy fit, an unfavorable strain range, and numerical errors. Instead of using the Birch-Murnaghan equation of state [28] for fitting, the **`ElaStic@exciting`** tool employs a more general polynomial fit [10]. The total energy, , in Eq. (2.39), dependent on the Lagrangian strain is approximated by polynomials up to order six

[5] `http://exciting-code.org/`

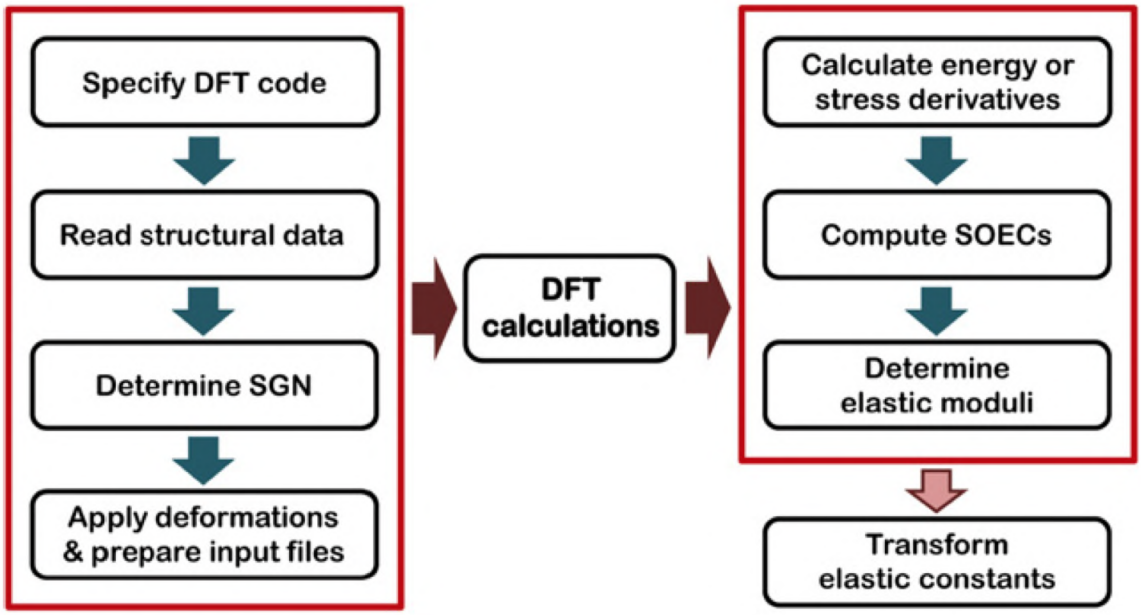

Figure 2.7: Flowchart for calculating second-order elastic constants using the **ElaStic@exciting** tool, taken from [10].

[10]

$$E(\eta) = \sum_{n=1}^{6} A_n \eta^n, \tag{2.76}$$

where A_n are constants. Note that the actual fit is done with a fixed order n. Due to the symmetric distribution of the strain points around the origin, polynomials of order $n+1$, where n is even, provide the same result as polynomials of order n [10]. Therefore, only polynomials of order 2, 4 and 6 have to be fitted. The second derivatives with respect to the strain η are then calculated by standard numerical techniques.

3 Results and Discussion

This Chapter will be dedicated to the results for the lattice parameters and second-order elastic constants.

3.1 Computational parameters

All calculations presented in this work were performed using the all-electron full-potential **exciting** code in the framework of the (L)APW+lo method [9]. The exchange and correlation energy term is treated by the generalized gradient approximation (GGA), in particular the PBEsol functional [25], which is said to have the highest accuracy in determining second-order elastic constants [29] among common exchange and correlation functionals. Atomic units are used for all calculations. For gallium the $1s^2$, $2s^2$ and $2p^6$ states were treated as core states and for oxygen the $1s^2$ state was treated as a core state. The choice of the particular energy parameters can be seen in the source files in Appendix A. All self-consistent ground-state calculations were converged to a total energy of less than 1 μHa. Results calculated with the optimized computational parameters show no noticeable changes for small changes of the muffin-tin radii for Gallium and Oxygen.

At the end of the groundstate calculation, an atomic relaxation at fixed lattice parameters is performed. For the α phase, a limited-memory version [30] of the Broyden–Fletcher–Goldfarb–Shanno bound constrained optimization method (labeled as **bfgs** in the **exciting** input), is used. If no convergence in the maximal force amplitude on the atoms up to $2 \cdot 10^{-4}$ Ha/a_0 can be reached by this method, additional relaxation will be done using the newton method, labeled as **newton**, where the atomic positions $\boldsymbol{R}_\alpha^{(q)}$ are updated according to

$$\boldsymbol{R}_\alpha^{(q+1)} = \boldsymbol{R}_\alpha^{(q)} + \varrho_\alpha^{(q)} \, (\boldsymbol{F}_\alpha^{(q)} + \boldsymbol{F}_\alpha^{(q-1)}), \tag{3.77}$$

with q representing the optimization step, $\boldsymbol{F}_\alpha^{(q)}$ the atomic forces, and $\varrho_\alpha^{(q)}$ the step size parameter. The atomic relaxation for the β phase is performed using the newton method with additional conditions specified for the atomic Cartesian coordinates, labeled as **harmonic** in the **exciting** code. The force threshold for convergence is $2 \cdot 10^{-4}$ Ha/a_0. For a more-in-depth description of the different relaxation methods in the **exciting** code, one is referred to the input reference manual on the web site[6] and Ref. [9].

3.2 Convergence tests

The calculation of elastic constants requires high accuracy in the computed equilibrium lattice constants. Therefore it is necessary to optimize the main computational

[6] `http://exciting-code.org/ref:input`

parameters, in order to achieve sufficient accuracy at reasonable computational cost.

The main computational parameters that have to be considered are the k-point mesh in reciprocal space and the value of $R_{\mathrm{MT}}^{\mathrm{min}} G_{\mathrm{max}}$, which represents the basis set size as shown in Section 2.3. Integrals are performed over the first Brillouin. The integrals are evaluated over a finite number of k points in each direction of the three basis vectors, called the k-point mesh. If the unit cell is large, the Brillouin zone will be small and only a small amount of k-points will be sufficient to approximate the integral in a computationally efficient way [31]. Therefore only a few k-points are necessary in directions of long basis vectors.

In order to do find adequate computational parameters, the fit parameters of the Birch-Murnaghan fit [28], the volume equilibrium V_0, bulk modulus B_0 and pressure derivative of the bulk modulus B_0', will be optimized. The subscript 0 represents the evaluation at zero pressure. While the Volume V_0 is dependent on the lattice parameters, the bulk modulus B_0 is a linear combination of second-order elastic constants, as shown in Section 2.1.5. The derivative of B_0 with respect to the pressure, B_0', is therefore a combination of second-order and third-order elastic constants. For the optimization, the energy-vs.-volume curve is created by applying a uniform physical strain with varying strength to the structure, *i.e.*, creating several deformed structures with slightly different volumes. The applied strain has the form

$$\boldsymbol{\epsilon} = \begin{pmatrix} 1+\varepsilon \\ 1+\varepsilon \\ 1+\varepsilon \\ 0 \\ 0 \\ 0 \end{pmatrix}, \tag{3.78}$$

where the parameter ε is chosen in the intervall $[-\varepsilon_{\mathrm{max}}, \varepsilon_{\mathrm{max}}]$. A total of 11 deformed structures are created for a strain interval $\varepsilon \in [-0.4, 0.4]$, where the strain points are equally spaced and symmetrically distributed around the origin. It is important to note that only the volume is optimized in this step and not all independent lattice parameters. However, for each volume, the atom positions are relaxed. The fit parameter B_0 is the bulk modulus when considering a uniform physical strain, therefore the calculated parameter B_0 is equivalent to the Voigt bulk modulus B_{V} introduced in Section 2.1.5.

3.2.1 Calculations for the α phase

The initial unit cell of Ga_2O_3 in the α phase is adopted from experiment in Ref. [7] and reduced to a primitive cell. The 3 primitive lattice vectors $a = b = 5.006\,\text{Å}$ and $c = 5.340\,\text{Å}$ have nearly the same length, and therefore it is reasonable to choose the same amount of k-points in each direction.

A convergence test of V_0, B_0, and B_0' with respect to $R_{\mathrm{MT}}^{\mathrm{min}} G_{\mathrm{max}}$ is performed on a 10×10×10 k-point mesh. The results of the convergence test can be seen in Table 3.1. A convergence up to $10^{-2}\,{a_0}^3$, $10^{-2}\,\text{GPa}$, and 10^{-2} for V_0, B_0, and B_0', respectively, is considered as sufficient and therefore further calculations will be done for $R_{\mathrm{MT}}^{\mathrm{min}} G_{\mathrm{max}} = 9.0$. Additionally the Birch-Murnaghan fit parameters are optimized with respect to the k-point mesh using $R_{\mathrm{MT}}^{\mathrm{min}} G_{\mathrm{max}} = 9.0$. The results are given in Table 3.2. A 8×8×8 k-point mesh yields convergence up to $10^{-3}\,{a_0}^3$, $10^{-3}\,\text{GPa}$, and 10^{-3} for V_0, B_0, and B_0', respectively, and is considered as sufficiently

Table 3.1: Convergence test with respect to $R_{\mathrm{MT}}^{\mathrm{min}} G_{\mathrm{max}}$ for the α phase of Ga_2O_3 using a 10×10×10 k-point mesh. The value picked for further calculations is marked by the green color.

$R_{\mathrm{MT}}^{\mathrm{min}} G_{\mathrm{max}}$	V_0 $[a_0{}^3]$	B_0 [GPa]	B_0'
7.0	656.09	219.79	4.513
8.0	656.74	218.30	4.489
9.0	657.04	218.07	4.459
10.0	657.07	218.09	4.453

Table 3.2: Convergence test with respect to the k-point mesh for the α phase of Ga_2O_3 using $R_{\mathrm{MT}}^{\mathrm{min}} G_{\mathrm{max}} = 9.0$. The mesh size picked for further calculations is marked by the green color.

k-point mesh	V_0 $[a_0{}^3]$	B_0 [GPa]	B_0'
4×4×4	657.0021	218.234	4.454
6×6×6	657.0428	218.075	4.457
8×8×8	657.0432	218.074	4.458
10×10×10	657.0421	218.067	4.459
12×12×12	656.0429	218.064	4.459
14×14×14	656.0420	218.069	4.459

accurate. Therefore, all further calculations for the α phase of Ga_2O_3 are performed using for $R_{\mathrm{MT}}^{\mathrm{min}} G_{\mathrm{max}} = 9.0$ and a 8×8×8 k-point mesh.

Table 3.3: Convergence test with respect to $R_{\mathrm{MT}}^{\mathrm{min}} G_{\mathrm{max}}$ for the β phase of Ga_2O_3 using a 2×8×4 k-point mesh. The value picked for further calculations is marked by the green color.

$R_{\mathrm{MT}}^{\mathrm{min}} G_{\mathrm{max}}$	V_0 [$a_0{}^3$]	B_0 [GPa]	B_0'
7.0	1425.79	197.87	4.489
8.0	1427.18	197.03	4.493
9.0	1427.61	196.90	4.486
10.0	1427.67	196.91	4.485

Table 3.4: Convergence test with respect to the k-point mesh for the β phase of Ga_2O_3 using $R_{\mathrm{MT}}^{\mathrm{min}} G_{\mathrm{max}} = 9.0$. The mesh size picked for further calculations is marked by the green color.

k-point mesh	V_0 [$a_0{}^3$]	B_0 [GPa]	B_0'
1×4×2	1427.167	197.48	4.482
2×8×4	1427.609	196.90	4.486
3×12×6	1427.634	196.89	4.483
4×16×8	1427.637	196.92	4.480
5×20×10	1427.637	196.92	4.480

3.2.2 Calculations for the β phase

The initial structure of Ga_2O_3 in the β phase is adopted from the experimental values in [5]. The lattice vectors have lengths of $a = 12.276$ Å, $b = 3.054$ Å, and $b = 5.816$ Å. The length of the reciprocal vectors is inverse proportional to the length of the respective lattice vector [31]. Therefore, the relation between the components of the reciprocal lattice vectors is $G_a < G_c < G_b$. Therefore, we choose less k-points in the directions of the lattice vectors $\boldsymbol{a}$ and $\boldsymbol{c}$. The results for different $R_{\mathrm{MT}}^{\mathrm{min}} G_{\mathrm{max}}$ values using a 2×8×4 k-point mesh are given in Table 3.3. Convergence with $R_{\mathrm{MT}}^{\mathrm{min}} G_{\mathrm{max}} = 9.0$ up to $10^{-2}\, a_0{}^3$, 10^{-2} GPa, and 10^{-3} for V_0, B_0, and B_0', respectively, are deemed sufficient. Using this value $R_{\mathrm{MT}}^{\mathrm{min}} G_{\mathrm{max}} = 9.0$, the optimization of the same parameters will be done with respect to the k-point mesh. The results are summarized in Table3.4. Using a 2×8×4 k-point mesh yields convergence up to $10^{-2}\, a_0{}^3$, 10^{-2} GPa, and 10^{-3} for V_0, B_0, and B_0', respectively. As a result, all further calculations for the β phase are performed with $R_{\mathrm{MT}}^{\mathrm{min}} G_{\mathrm{max}} = 9.0$ on a 2×8×4 k-point mesh.

3.3 Lattice optimization

In the previous Section, the most important convergence parameters were obtained by checking their influence on the parameters of the Birch-Murnaghan fit. Now the lattice parameters of both phases at zero pressure will be optimized. This optimization is essential because second-order elastic constants describe the linear relation between strain and stress acting on a solid. A change in the structure equals a change in the second-order elastic constants. Therefore, the lattice parameters have to be optimized because the second-order elastic constants are calculated from the equilibrium structure. Thereby internal relaxation of the atoms is done analogous to Section 3.2.

The unit cell of an arbitrary crystal is determined by 6 lattice parameters, a, b, c, α, β and γ. The first three represent the lengths of the vectors spanning the unit cell and the last three represent the angles between them. Optimizing the crystal with respect to all parameters can be done using an iterative scheme, where in each step only one parameter is varied while the others are fixed. In the case of the rhombohedral α phase of Ga_2O_3 with hexagonal axes, only the lattice vectores a and c have to be optimized, and the iterative scheme has the form [31]:

Step 1: Minimization with respect to the volume V (applying a uniform strain, all other parameters fixed),

Step 2: Minimization with respect to the ratio c/a (all other parameters fixed).

In the monoclinic β phase a, b, c and the angle β between $\boldsymbol{a}$ and $\boldsymbol{c}$ have to be optimized and therefore the scheme takes on the form:

Step 1: Minimization with respect to the volume V (applying a uniform strain, all other parameters fixed),

Step 2: Minimization with respect to the ratio b/a (all other parameters fixed),

Step 3: Minimization with respect to the ratio c/a (all other parameters fixed),

Step 4: Minimization with respect to the angle β between $\boldsymbol{a}$ and $\boldsymbol{c}$ (all other parameters fixed).

The physical strain tensors $\boldsymbol{\epsilon}$ corresponding to these optimization steps are:

$$\text{Volume } V\text{:}\quad \boldsymbol{T}_V = \begin{pmatrix} 1+\varepsilon \\ 1+\varepsilon \\ 1+\varepsilon \\ 0 \\ 0 \\ 0 \end{pmatrix} \qquad \text{Ratio } b/a\text{:}\quad \boldsymbol{T}_{b/a} = \begin{pmatrix} (1+\varepsilon)^{-1/2} \\ 1+\varepsilon \\ (1+\varepsilon)^{-1/2} \\ 0 \\ 0 \\ 0 \end{pmatrix}$$

$$\text{Ratio } c/a\text{:}\quad \boldsymbol{T}_{c/a} = \begin{pmatrix} (1+\varepsilon)^{-1/2} \\ (1+\varepsilon)^{-1/2} \\ 1+\varepsilon \\ 0 \\ 0 \\ 0 \end{pmatrix} \qquad \text{Angle } \beta\text{:}\quad \boldsymbol{T}_{\beta} = \begin{pmatrix} 1 \\ 1/(1-\varepsilon^2) \\ 1 \\ 0 \\ \varepsilon \\ 0 \end{pmatrix}$$

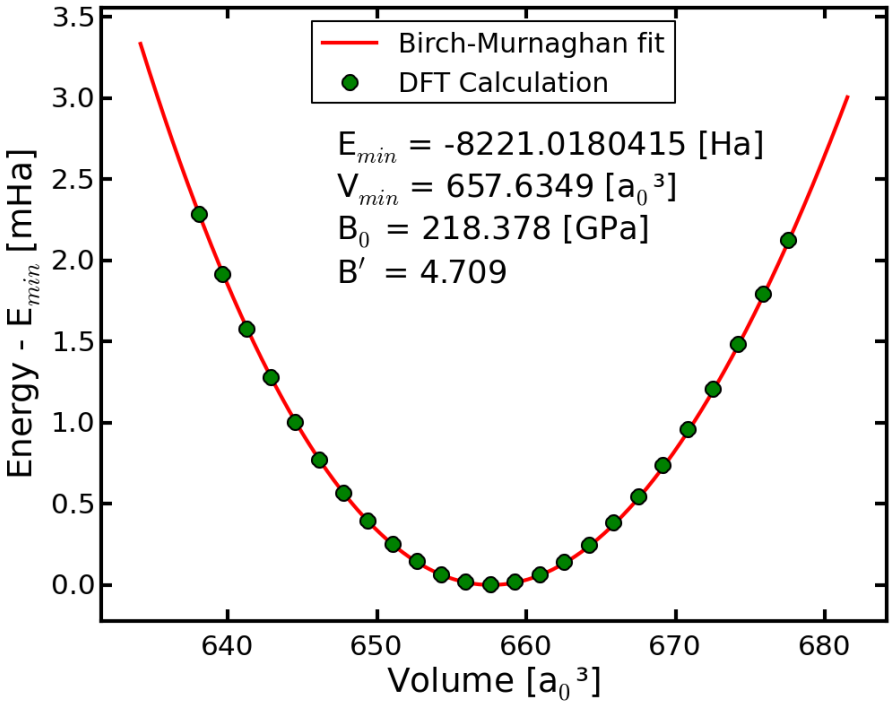

Figure 3.8: Calculated energy-vs.-volume curve with Birch-Murnaghan fit for substep 1 of the final optimization step of Ga_2O_3 in the α phase.

One optimization step combines all the substeps of the iterative sheme.

Energy-vs.-volume and energy-vs.-strain curves are derived for a defined number n of deformed structures in the interval $\varepsilon \in [-\varepsilon_{\max}, \varepsilon_{\max}]$. Note that the strain points are equally spaced and symmetrically distributed around the origin. The optimized lattice parameters are obtained from the minimum of the energy fit.

An example of the lattice optimization procedure, the final optimization step of Ga_2O_3 in the α phase, is given in Figures 3.8 and 3.9.

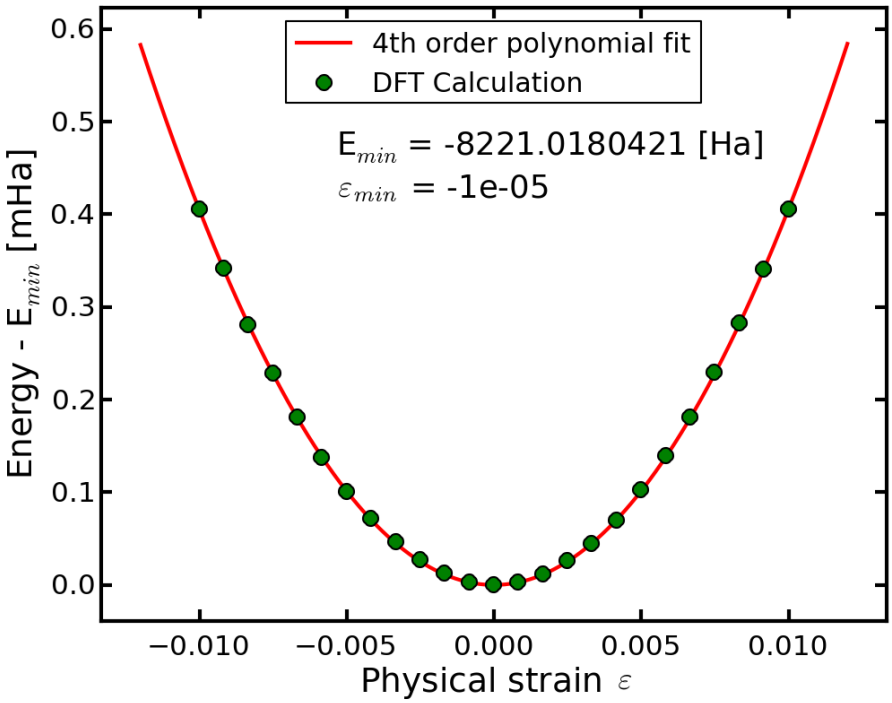

Figure 3.9: Calculated energy-vs.-strain curve with fourth-order polynomial fit for substep 2 of the final optimization step of Ga_2O_3 in the α phase.

3.3.1 Calculations for the α phase

The convergence of the lattice parameters and bulk modulus B_0 with respect to the optimization steps can be found in Table 3.5. The bulk modulus and its pressure derivative converged to 10^{-2} GPa and 10^{-2}, respectively, while the lattice parameters converged to more than 10^{-3} Å.

In order to compare the calculated primitive lattice parameters with the experimental conventional lattice parameters, the following transformation has to be applied:

$$a_{\text{corundum}} = a \tag{3.79}$$

$$c_{\text{corundum}} = 3 \cdot c_z, \tag{3.80}$$

where c_z represents the z component of the calculated primitive lattice vector $\boldsymbol{c}$. This can be understood by repeating the primitive unit cell in Fig. 1.2 a total of three times in the z direction. The calculated lattice parameters show excellent agreement with other theoretical and experimental results, shown in Table 3.6 while the difference in the bulk modulus B_0 compared to the experimental value is about 10 to 20 %, which is expected for a DFT calculation of elastic properties [12]. There is a slight overestimation of the calculated lattice parameters compared to the experimental values of 1.4 % and 0.3 % for a and c, respectively.

Table 3.5: Convergence of lattice parameters and bulk modulus B_0 of Ga_2O_3 in the α at zero pressure. The maximum strain parameter ε_{max} and the number of deformed structures n is given for each optimization step.

Optimization step	a [Å]	c [Å]	B_0 [GPa]	B_0'
1: $\varepsilon_{max} = 0.04$; $n = 11$	5.006	5.340	218.26	4.46
2: $\varepsilon_{max} = 0.01$; $n = 11$	5.006	5.340	218.39	4.72
3: $\varepsilon_{max} = 0.01$; $n = 17$	5.006	5.340	218.41	4.72
4: $\varepsilon_{max} = 0.01$; $n = 25$	5.006	5.340	218.38	4.71

Table 3.6: Comparison of calculated lattice parameters and bulk modulus of Ga_2O_3 in the α phase at zero pressure with experimental and other theoretical results. The used exchange and correlation functional is given in parentheses.

	$a_{corundum}$ [Å]	$c_{corundum}$ [Å]	B_0 [GPa]	B_0'
Present work (GGA)	5.006	13.471	218.38	4.71
Theory [32] (B3LYP)	5.04	13.56	210	4.95
Theory [33] (LDA)	4.952	13.319	243.66	3.81
Theory [34] (GGA)	5.059	13.62		
Experiment [7]	4.983	13.43		
Experiment [4]	4.979	13.432	252 (14)	4

3.3.2 Calculations for the β phase

The results of the optimization process can be found in Table 3.7. The lattice parameters, the bulk modulus and its pressure derivative were converged to 10^{-3} Å, 10^{-2} GPa and 10^{-1}, respectively. The calculated lattice parameters are in very good agreement with former experimental and theoretical results, see Table 3.8, although they are slightly overestimated by 0.3 % on average. The difference of the calculated bulk modulus compared to the experimental value is about 10 %, and therefore well within the expected accuracy. The optimized structure for the β phase can be seen in Fig. 1.1.

Table 3.7: Convergence of lattice parameters and bulk modulus B_0 of Ga_2O_3 in the β at zero pressure. The maximum strain parameter $\varepsilon_{\max}$ and the number of deformed structures n is given for each optimization step.

Optimization step	a [Å]	b [Å]	c [Å]	β [°]	B_0 [GPa]	B_0'
1: $\varepsilon_{\max} = 0.04$; $n = 11$	12.276	3.054	5.816	103.74	169.00	3.96
2: $\varepsilon_{\max} = 0.01$; $n = 11$	12.293	3.052	5.813	103.73	168.63	3.78
3: $\varepsilon_{\max} = 0.01$; $n = 15$	12.303	3.045	5.813	103.72	168.54	3.60
4: $\varepsilon_{\max} = 0.01$; $n = 15$	12.308	3.050	5.812	103.71	168.59	3.70

Table 3.8: Comparison of calculated lattice parameters and bulk modulus of Ga_2O_3 in the β phase at zero pressure with experimental and other theoretical results. The used exchange and correlation functional is given in parentheses.

	a [Å]	b [Å]	c [Å]	β [°]	B_0 [GPa]	B_0'
Present work (GGA)	12.308	3.050	5.812	103.71	168.59	3.70
Theory [32] (B3LYP)	12.34	3.08	5.87	103.9	174	3.79
Theory [32] (LDA)	12.208	3.031	5.751	103.63	218.57	3.153
Theory [32] (GGA)	12.438	3.084	5.877	103.71		
Experiment [5]	12.23	3.04	5.80	103.7		
Experiment [4]	12.23	3.04	5.80	103.82	184.4(3)	4

3.4 Elastic constants

This section is dedicated to the calculation of the second-order elastic constants of the α and β phase of Ga_2O_3 using the **`ElaStic@exciting`** code, described in Section 2.4. The second-order elastic constants are derived by numerically calculating the energy derivatives in Eq. (2.41) between multiple deformed structures. The minimum amount of different deformation types that have to be applied to a material has to be equal to the number of independent second-order elastic constants, see Section 2.1.2. When the deformation types are chosen properly, a system of linear equations can be solved for calculating the second-order elastic constants.

In order to illustrate the evaluation of the energy derivatives, an example for a uniform strain in the form $\boldsymbol{\eta}^{(i)} = (\eta, \eta, \eta, 0, 0, 0)$ applied on the α structure of Ga_2O_3 is given in Figures 3.10 and 3.11. The energy and second derivative of the energy with respect to the strain are calculated for a strain $\eta \in [-0.03, 0.03]$ using a total of 41 strain points. This procedure is repeated for $\eta \in [-\eta_{\max}, \eta_{\max}]$ with $\eta_{\max} \leq 0.03$, and using the same density of strain points. A general guideline for finding the correct value for the numerical derivative of the energy is, to find the region where the polynomial fit shows a plateau in the displayed region of the maximum applied strain $\eta_{\max}$. Assume that the calculated energy is exactly given by a polynomial of order n. Then the second derivative of the energy with respect to the strain is a constant when evaluated at zero strain. This is only be valid if the energy was calculated without any numerical noise. Although a DFT calculation always has numerical uncertainties, the general idea of finding plateaus in the displayed

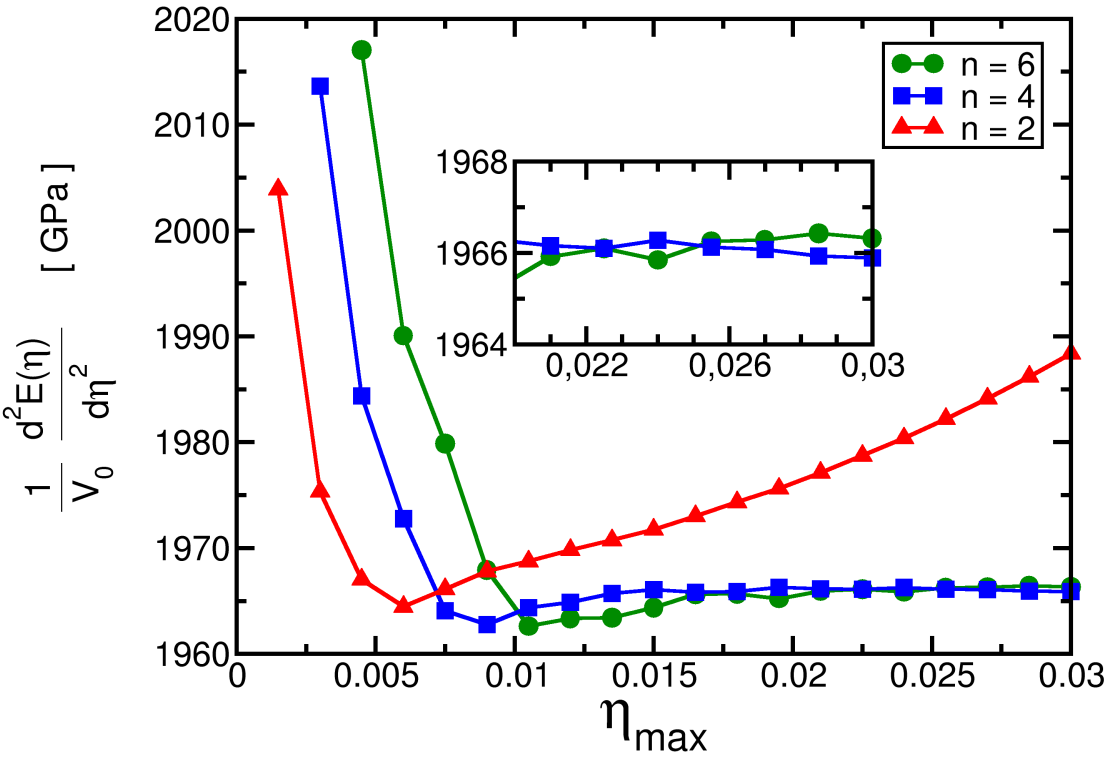

Figure 3.10: Energy derivative-vs.-strain curve for uniform strain fitted with the polynomial method for the α phase of Ga_2O_3, with n the order of the polynomial. The inset shows the plateu region of the fitted curves. Note that the labels of the inset have the same units as the graph.

region is still valid. For small values of $\eta_{\max}$ and a small number of strain points, a polynomial fit with lower order is generally best. If higher $\eta_{\max}$ values are chosen, then higher polynomial fits are normally better. A more detailed discussion on the accuracy of the method is given in [10].

Applying this concept to Fig. 3.10, yields a result for the energy derivative of about $\frac{1}{V_0}\frac{\partial^2 E}{\partial \eta^2} \approx 1966\,\text{GPa}$ at a maximum strain $\eta_{\max} = 0.025$.

3.4.1 Calculations for the α phase

The stiffness tensor $\boldsymbol{C}_\alpha$ of the rhombohedral α phase has 6 independant components and can be written in Voigt notation as [16]:

$$\boldsymbol{C}_\alpha = \begin{pmatrix} C_{11} & C_{12} & C_{13} & C_{14} & 0 & 0 \\ C_{12} & C_{11} & C_{13} & -C_{14} & 0 & 0 \\ C_{13} & C_{13} & C_{33} & 0 & 0 & 0 \\ C_{14} & -C_{14} & 0 & C_{44} & 0 & 0 \\ 0 & 0 & 0 & 0 & C_{44} & C_{14} \\ 0 & 0 & 0 & 0 & C_{14} & \frac{1}{2}(C_{11} - C_{12}) \end{pmatrix}. \tag{3.81}$$

For the calculation of the elastic constants of the α phase, it is therefore necessary to apply at least 6 different deformation types to the structure. A suitable combination of deformations, implemented in the **`ElaStic@exciting`** code, is given in Table 3.9. For every deformation type, 41 equally spaced strain points, that are symmetrically

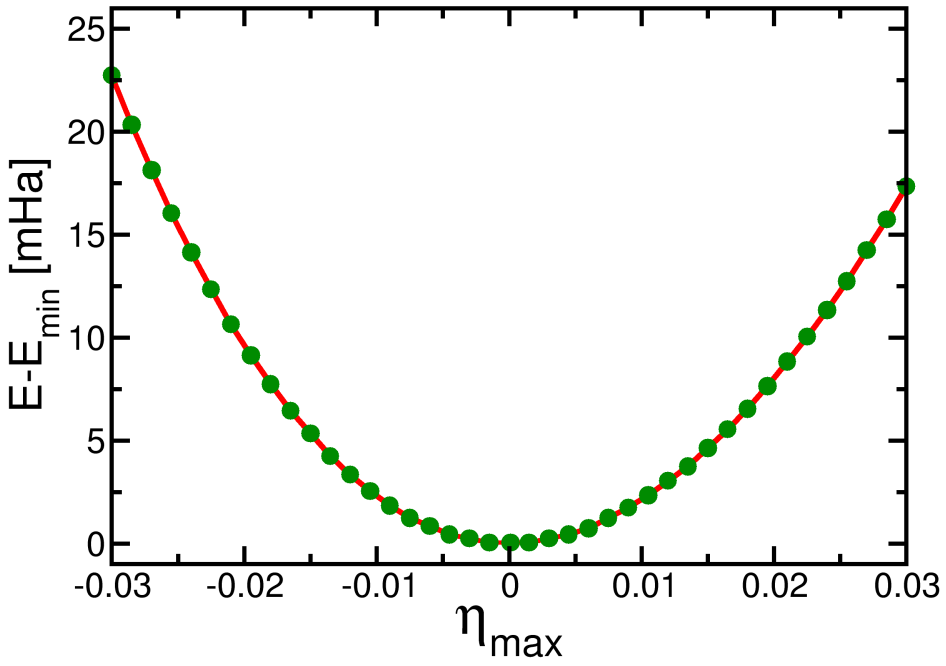

Figure 3.11: Energy-vs.strain curve for uniform strain of the α phase of Ga_2O_3 for a total of 41 deformed structures.

distributed around the origin, are created for $\eta \in [-\eta_{\max}, \eta_{\max}]$ with $\eta_{\max} \leq 0.03$. The energy is calculated by the **exciting** code. Afterwards the energy derivative is numerically calculated by using a polynomial fit. For all deformation types, every energy derivative-vs.-strain curve has to be examined and the respective plateaus within the region of the maximum strain parameter $\eta_{\max}$ have to be located. The second-order elastic constants can then be calculated by solving the obtained system of linear equations. The energy derivative-vs-strain curves can be found in Figures 3.10, 3.13, 3.14 and 3.15. The calculated second-order elastic constants and elastic moduli(see Section2.1.5) for the α phase of Ga_2O_3 can be found in Table3.10 and3.11, respectively. To the best of the authors knowledge, there are no experimental or theoretical results available. Only the bulk modulus B_V has been calculated in theoretical and experimental works by using the Birch-Murnaghan fit, and a comparison with this work can be found in Table 3.12. The absolute difference between the Voigt bulk moduli calculated in Section 3.3.1 and this Section is 0.05 GPa and therefore show excellent agreement. The relative difference in comparison to other results is like before about 10 %.

Table 3.9: Applied deformation types $\boldsymbol{\eta}^{(i)}$ for the α phase of Ga_2O_3, as implemented in **ElaStic** [10]. The Lagrangian strain in Voigt notation is given as a vector $\boldsymbol{\eta}^{(i)} = (\eta_1, \eta_2, \eta_3, \eta_4, \eta_5, \eta_6)$.

$\boldsymbol{\eta}^{(i)}$	η_1	η_2	η_3	η_4	η_5	η_6
$\boldsymbol{\eta}^{(1)}$	η	η	η	0	0	0
$\boldsymbol{\eta}^{(2)}$	η	η	0	0	0	0
$\boldsymbol{\eta}^{(3)}$	0	0	η	0	0	0
$\boldsymbol{\eta}^{(4)}$	η	0	0	0	0	0
$\boldsymbol{\eta}^{(5)}$	0	0	0	2η	0	0
$\boldsymbol{\eta}^{(6)}$	η	0	0	2η	0	0

Table 3.10: Calculated independent second-order elastic constants (in GPa) and compliances (in GPa^{-1}) of the α phase of Ga_2O_3.

C_{ij}	[GPa]	S_{ij}	[GPa^{-1}]
C_{11}	380.3	S_{11}	0.00360
C_{12}	174.4	S_{12}	−0.00142
C_{13}	128.4	S_{13}	−0.00082
C_{14}	16.5	S_{14}	−0.00104
C_{33}	343.0	S_{33}	0.00353
C_{44}	79.9	S_{44}	0.01294

Table 3.12: Comparison of the calculated Voigt bulk moduli B_0, as a linear combination of the calculated second-order elastic constants (SOEC) and parameter of the Birch-Murnaghan equation of state (BM), at zero pressure for the α phase of Ga_2O_3 with other theoretical and experimental results. The exchange correlation is given in parentheses.

	B_V [GPa]
Present work (GGA), BM	218.38
Present work (GGA), SOEC	218.43
Theory [32] (B3LYP), BM	210
Theory [33] (LDA), BM	243.66
Experiment [4], BM	252(14)

Table 3.11: Elastic moduli (in GPa) of the α phase of Ga_2O_3 and Poisson ratios for different notations as described in Section 2.1.5.

	B [GPa]	G [GPa]	E [GPa]	ν [GPa]
Voigt	218.43	97.40	254.40	0.31
Reuss	216.31	92.08	241.92	0.31
Hill	217.37	94.74	248.17	0.31

Table 3.13: Applied deformation types $\boldsymbol{\eta}^{(i)}$ for the β phase of Ga_2O_3, implemented in `ElaStic` [10]. The Lagrangian strain in Voigt notation is given as a vector $\boldsymbol{\eta}^{(i)} = (\eta_1, \eta_2, \eta_3, \eta_4, \eta_5, \eta_6)$.

$\boldsymbol{\eta}^{(i)}$	η_1	η_2	η_3	η_4	η_5	η_6
$\boldsymbol{\eta}^{(1)}$	η	η	η	0	0	0
$\boldsymbol{\eta}^{(2)}$	$\frac{1}{2}\eta$	$-\eta$	$\frac{1}{2}\eta$	0	0	0
$\boldsymbol{\eta}^{(3)}$	$-\eta$	$\frac{1}{2}\eta$	$\frac{1}{2}\eta$	0	0	0
$\boldsymbol{\eta}^{(4)}$	η	$-\eta$	0	0	0	2η
$\boldsymbol{\eta}^{(5)}$	0	η	$-\eta$	0	0	2η
$\boldsymbol{\eta}^{(6)}$	η	$-\eta$	0	0	0	0
$\boldsymbol{\eta}^{(7)}$	0	0	0	2η	2η	0
$\boldsymbol{\eta}^{(8)}$	η	0	0	0	0	2η
$\boldsymbol{\eta}^{(9)}$	0	η	0	0	0	0
$\boldsymbol{\eta}^{(10)}$	0	0	η	0	0	0
$\boldsymbol{\eta}^{(11)}$	0	0	0	2η	0	0
$\boldsymbol{\eta}^{(12)}$	0	0	0	0	2η	0
$\boldsymbol{\eta}^{(13)}$	0	0	0	0	0	2η

3.4.2 Calculations for the β phase

The stiffness tensor $\boldsymbol{C}_\beta$ of the monoclinic β phase has 13 independant components and can be written in Voigt notation as [16]:

$$\boldsymbol{C}_\alpha = \begin{pmatrix} C_{11} & C_{12} & C_{13} & 0 & 0 & C_{16} \\ C_{12} & C_{22} & C_{23} & 0 & 0 & C_{26} \\ C_{13} & C_{23} & C_{33} & 0 & 0 & C_{36} \\ 0 & 0 & 0 & C_{44} & C_{45} & 0 \\ 0 & 0 & 0 & C_{45} & C_{55} & 0 \\ C_{16} & C_{26} & C_{36} & 0 & 0 & C_{66} \end{pmatrix}. \tag{3.82}$$

Therefore, a minimum of 13 deformation types has to be chosen. A satisfactory set of deformations implemented in the `ElaStic@exciting` code is found in Table 3.13. The calculations for the monoclinic β phase are a lot more computationally demanding due to the low crystal symmetry and high number (20) of atoms in the unit cell. Therefore, only 31 equally spaced strain points, around the origin, are created for a strain $\eta \in [-\eta_{\max}, \eta_{\max}]$ with $\eta_{\max} \leq 0.03$. Analogous to the previous calculations for the α phase, the plateau regions for every energy derivative-vs.-strain curve have to be located. Due to limited time, only 9 independent second-order elastic constants

Table 3.14: The 9 calculated independent second-order elastic constants (in GPa) and the elastic moduli (in GPa) in Voigt notation.

C_{11}	C_{12}	C_{13}	C_{22}	C_{23}	C_{33}	C_{44}	C_{55}	C_{66}	B_V	G_V	E_V	ν_V
227.8	119.7	137.7	327.6	76.5	319.6	49.9	66.2	91.5	171.4	77.6	202.3	0.3

have been calculated so far. The resulting graphs can be found in Figure 16 and in Appendix B. The 9 calculated second-order elastic constants and a comparison of the calculated Voigt elastic moduli with previous and experimental results can be found in Tables 3.14 and 3.15.

Table 3.15: Comparison of the calculated Voigt bulk moduli B_V, as a linear combination of the calculated second-order elastic constants (SOEC) and parameter of the Birch-Murnaghan equation of state (BM), at zero pressure for the β phase of Ga_2O_3 with other theoretical and experimental results. The exchange correlation is given in brackets.

	B_V [GPa]
Present work (GGA), BM	168.59
Present work (GGA), SOEC	171.42
Theory [32] (B3LYP), BM	174
Theory [33] (LDA), BM	218.57
Experiment [4], BM	184.4(3)

The calculated Voigt bulk moduli B_V of this Section and Section 3.3.2 are in good agreement with one another and other experimental and theoretical results, as seen in Table 3.15. The relative difference between B_V calculated with the Birch-Murnaghan fit and the second-order elastic constants is less than 2 %. Higher accuracy could be achieved by considering more than 31 strain points. The calculated bulk moduli differ by less than 10 % compared to the experimental result. A comparison of elastic constants between the α and β phase can be found in Table 3.16. The calculated bulk modulus B_V for the α phase is higher than for the β phase. This is consistent with previous results as well as experimental results, see Tables 3.7 and 3.6.

3.5 Phase stability

The calculation of the second-order elastic constants and therefore the stiffness tensor $\boldsymbol{C}$ enables the investigation of the elastic stability of solids. It is known that the β phase is thermodynamically stable at ambient conditions while the α phase is metastable. Experiments have shown that a phase transition from the β to the α phase occurs below 10 GPa hydrostatic pressure [4] which has also been stated in theoretical results [32].

General elastic stability conditions have first been proposed by Born [35]. In the harmonic approximation and if no strain is present, a crystalline structure is only stable, if for all phonon modes $\omega^2(\boldsymbol{q}, s) > 0$ is valid and the elastic energy, defined in

Table 3.16: Calculated independent second-order elastic constants (in GPa) and Voigt bulk moduli (in GPa) of the α and β phase of Ga_2O_3. The Voigt bulk moduli were calculated using a linear combination of second-order elastic constants (SOEC) and a Birch-Murnaghan fit (BM).

α phase		β phase	
C_{11}	380.3	C_{11}	227.8
C_{12}	174.4	C_{12}	119.7
C_{13}	128.4	C_{13}	137.7
C_{14}	16.5	C_{22}	327.6
C_{33}	343.0	C_{23}	76.5
C_{44}	79.9	C_{33}	319.6
		C_{44}	49.9
		C_{55}	66.2
		C_{66}	91.5
B_V, BM	218.4	B_V, BM	168.6
B_V, SOEC	218.4	B_V, SOEC	171.4

Table 3.17: Eigenvalues λ_i (in GPa) of the stiffness tensor $\boldsymbol{C}$ for the α phase of Ga_2O_3, given in Voigt notation.

Phase	λ_1	λ_2	λ_3	λ_4	λ_5	λ_6
α	659.0	75.7	210.2	238.7	71.3	111.6

Eq. 2.24, is always positive for all $\boldsymbol{\epsilon} \neq 0$. $\omega(\boldsymbol{q}, s)$ refers to the phonon frequency, $\boldsymbol{q}$ tp the wavevector, and s to the polarization and phonon branches. A mathematical equivalent expression of these two conditions is that the eigenvalues of the stiffness tensor $\boldsymbol{C}$ have to be positive [36].

The second-order elastic constants were calculated at zero stress using Eq. 2.41. In order to have elastic stability, the eigenvalues of the stifness tensor have to positive. They are calculated by standard linear algebra routines. The results are given in Table 3.17. All eigenvalues are positive for the α phase and therefore, it is elastically stable at equilibrium for zero strain. This coincides with experimental results, where The calculation of the eigenvalues for the β phase was not possible due to missing components in the stiffness tensor. However, we can say that the α resists volume compression more than the β phase, due to a higher bulk modulus B_V. Also, the Young modulus E_V is higher for α phase corresponding to higher resistance to unaxial strain. The higher shear modulus G_V of the α phase means higher resistance elastic deformations in a direction of the applied strain. The α phase is therefore harder, if you consider hardness scales with the elastic moduli [37, 38]. It is known that hydrostatic pressure induces a phase transition from the α to the β phase [4]. A lower bulk modulus and therefore, less resistance against uniform compression, could be an indicator as to why this phase transition occurs. If one wants to examine this transition further, one has to investigate elastic stability under an arbitrary stress $\boldsymbol{\sigma}$. Then the Born criterion has to be examined by using the elastic stiffness tensor under load $\boldsymbol{B}$ instead of the stiffness tensor [39].

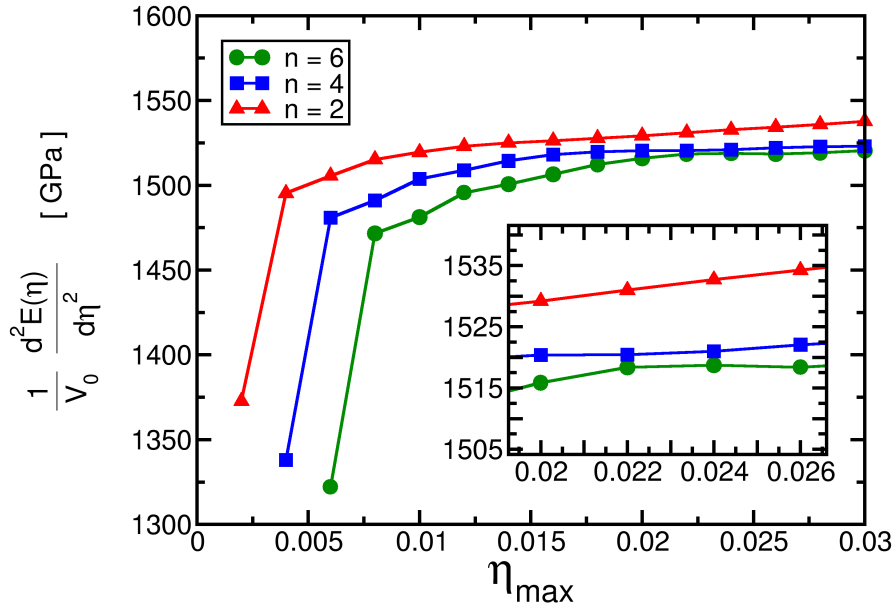

Figure 3.12: Energy derivative-vs.-strain curve as obtained from total-energy calculations (dots) and a corresponding polynomial fit of order n (solid line) for the β phase of Ga_2O_3, with n the order of the polynomial. The applied Lagrangian strain tensor is $\boldsymbol{\eta} = (\eta, \eta, \eta, 0, 0, 0)$ in Voigt notation.

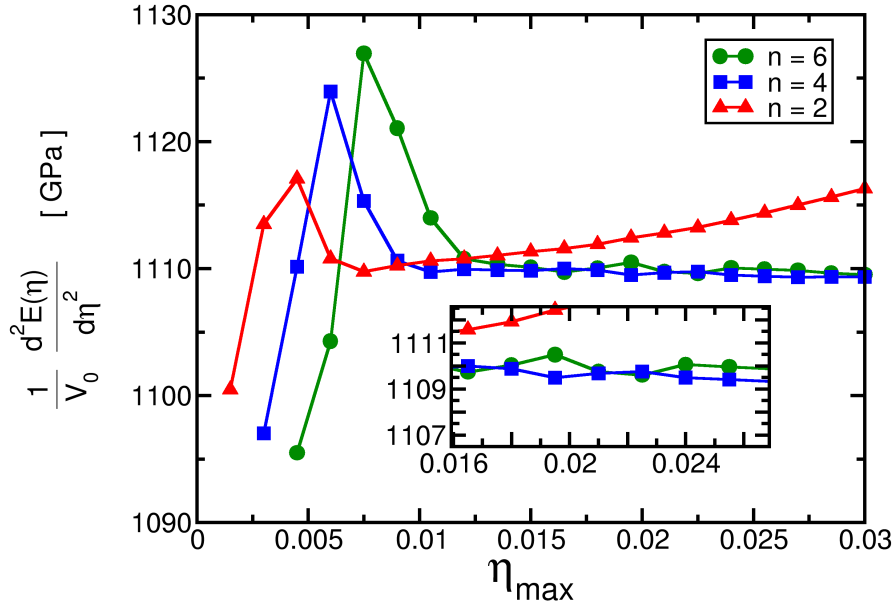

Figure 3.13: Energy derivative-vs.-strain curve as obtained from total-energy calculations (dots) and a corresponding polynomial fit of order n (solid line) for the α phase of Ga_2O_3, with n the order of the polynomial. The applied Lagrangian strain tensor is $\boldsymbol{\eta} = (\eta, \eta, 0, 0, 0, 0)$ in Voigt notation.

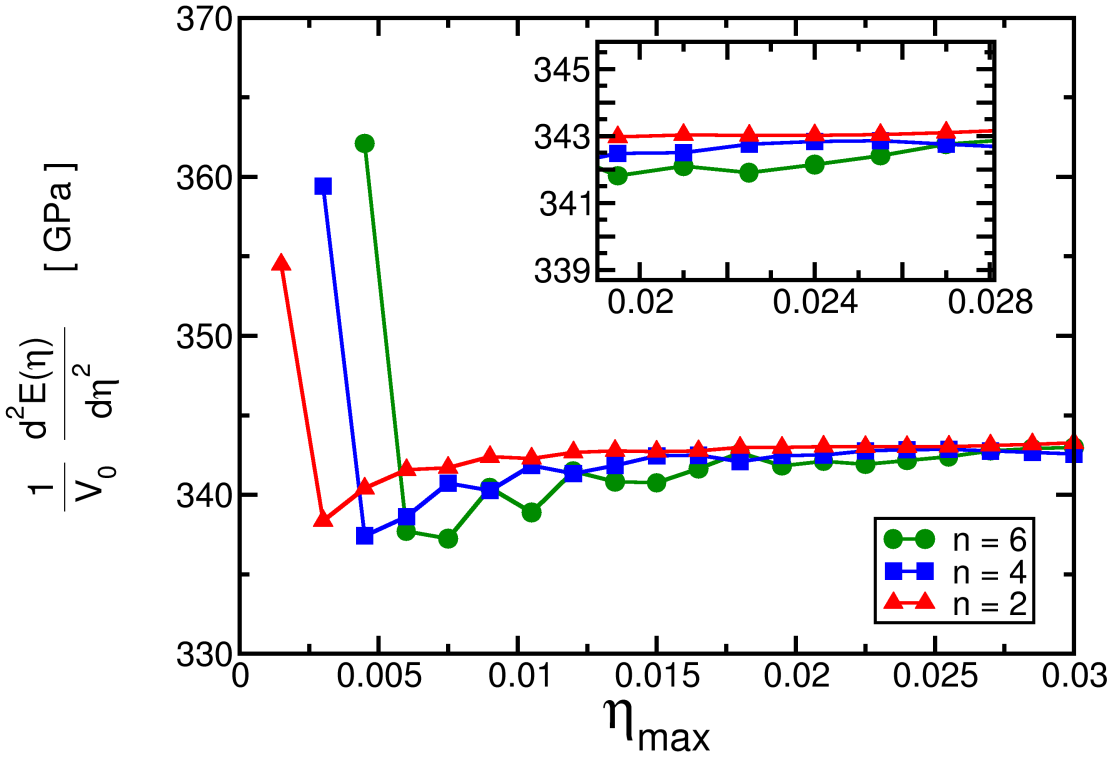

(a) $\boldsymbol{\eta} = (0, 0, \eta, 0, 0, 0)$

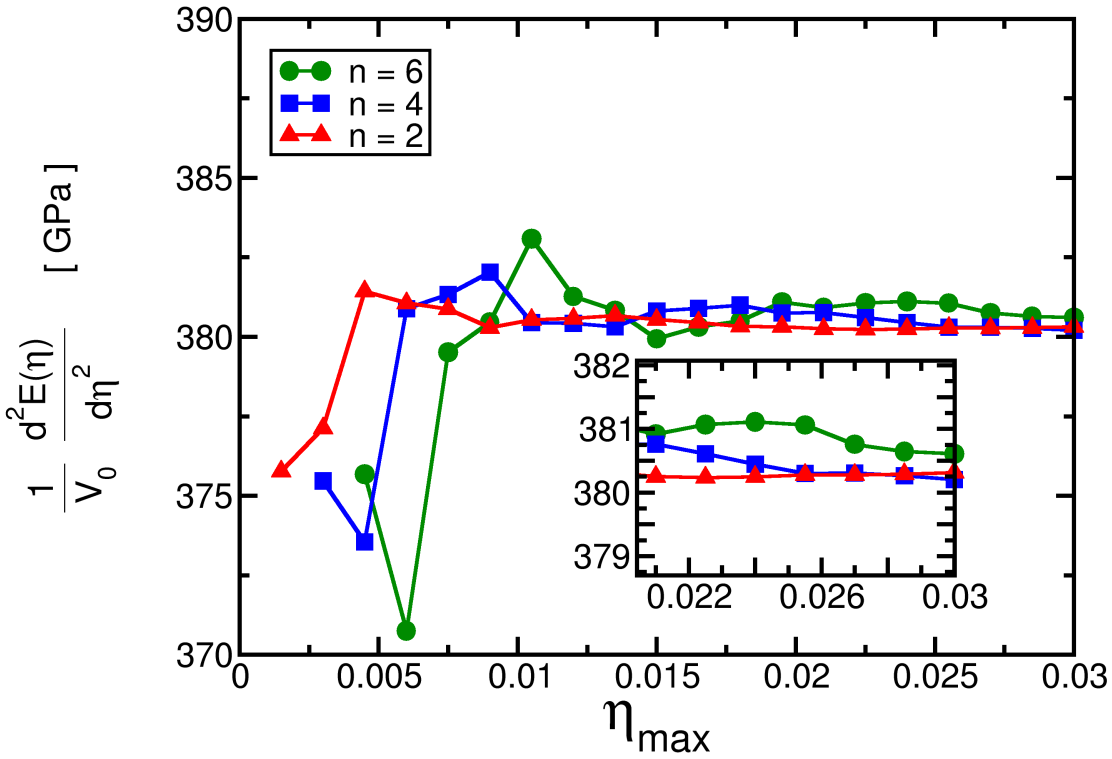

(b) $\boldsymbol{\eta} = (\eta, 0, 0, 0, 0, 0)$

Figure 3.14: Same as Fig 3.13 with the strain tensor specified in (a) and (b).

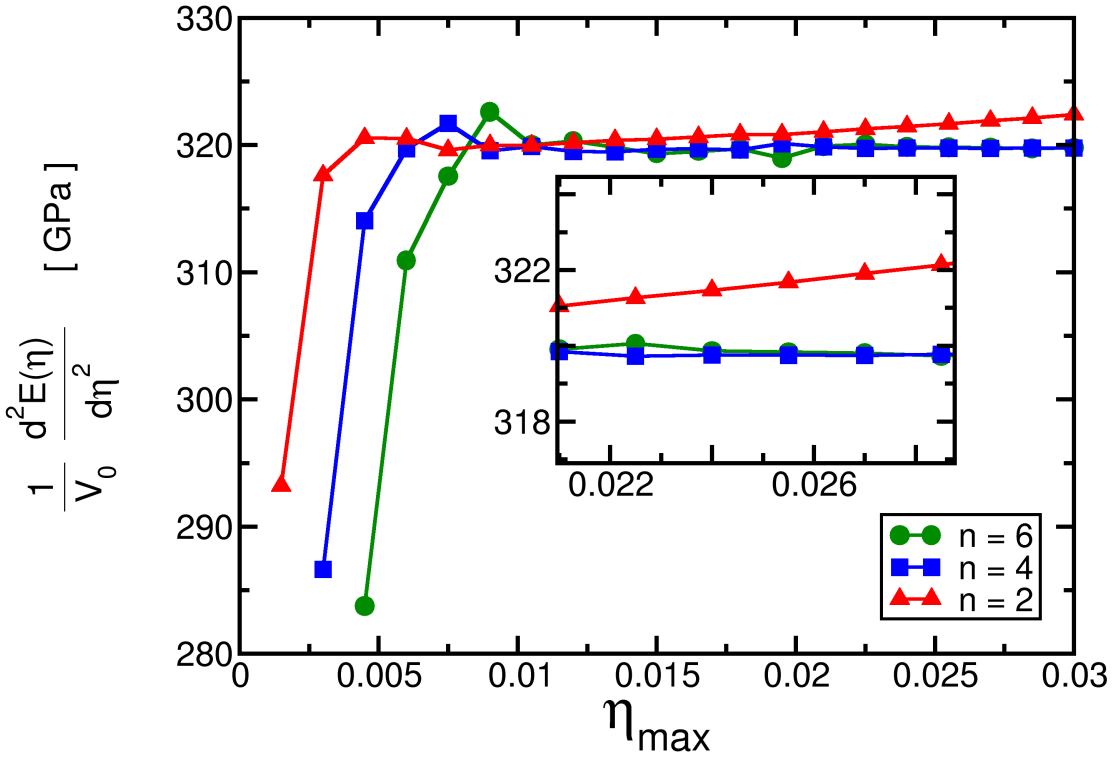

(a) $\boldsymbol{\eta} = (0, 0, 0, 2\eta, 0, 0)$

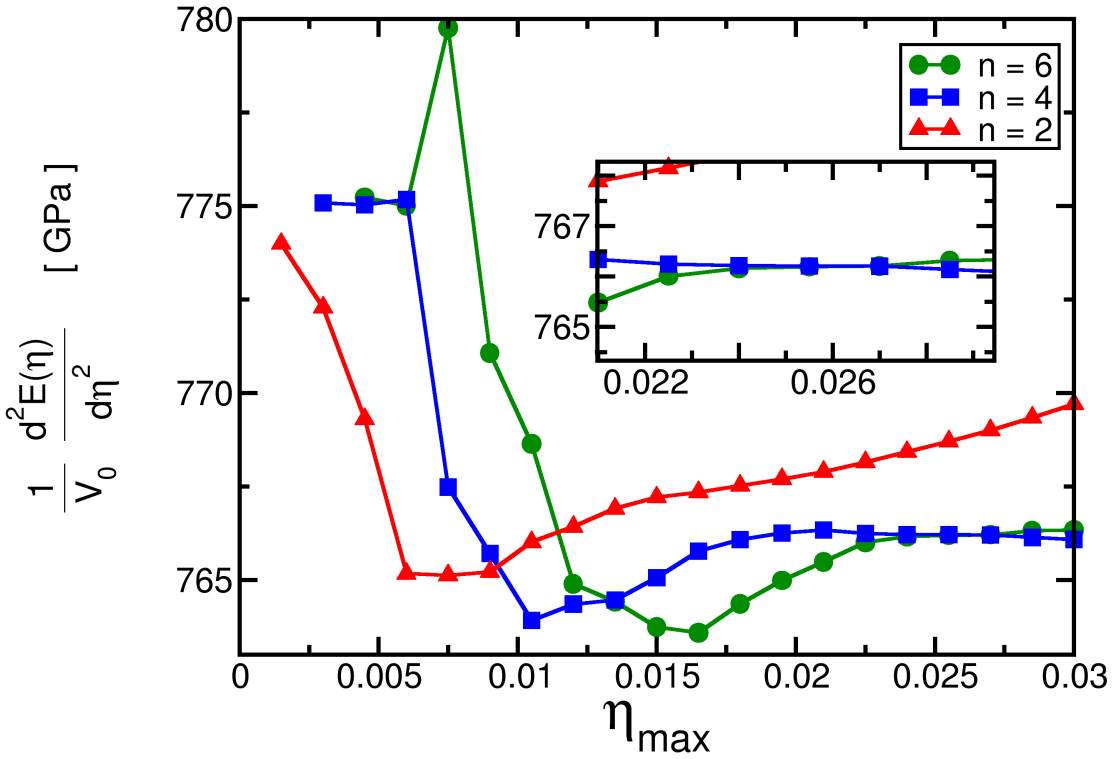

(b) $\boldsymbol{\eta} = (\eta, 0, 0, 2\eta, 0, 0)$

Figure 3.15: Same as Fig. 3.13 with the strain tensor specified in (a) and (b).

4 Conclusions and Outlook

In this work, the lattice parameters and elastic properties of the rhombohedral α and monoclinic β phase of Ga_2O_3 were calculated from first principles using the full-potential all-electron **exciting** code and the **ElaStic@exciting** tool.

Calculations for both phases were performed with the (L)APW+lo basis set using a generalized gradient approximation (PBEsol) functional as an approximation for the exchange and correlation functional. The optimized values of the main computational parameters k-point mesh and $R_{\mathrm{MT}}^{\mathrm{min}} G_{\mathrm{max}}$ for the α and β phase were 8×8×8 and $R_{\mathrm{MT}}^{\mathrm{min}} G_{\mathrm{max}} = 9.0$, and 2×8×4 and $R_{\mathrm{MT}}^{\mathrm{min}} G_{\mathrm{max}} = 9.0$, respectively.

The optimized lattice parameters for the α phase of $a = 5.006\,\text{Å}$ and $c = 13.471\,\text{Å}$ are in very good agreement with experimental results although they are overestimating the lattice parameters by 1.4 % and 0.3 % for a and c, respectively. The same holds true for the β phase, where the optimized values $a = 12.308\,\text{Å}$, $b = 3.050\,\text{Å}$, $c = 5.812\,\text{Å}$, and $\beta = 103.71°$ are overestimated by an average of 0.3 %. This is a common result when using GGA functionals for the exchange and correlation functional [40].

Calculations of the second-order elastic constants were performed using a polynomial -fit method, implemented in the **ElaStic@exciting** tool. A total of 41 and 31 strain points were created for a maximum strain of 0.03 for the α and β phase, respectively. Note that for the β phase only 9 independent elastic constants were calculated due to insufficient time. The results can be found in Table 3.16.

The two calculated bulk moduli for both phases are in good agreement with each other and differ about 10 % compared to the experimental results. When comparing these results with experimental results, it is important to note that the second-order elastic constants are dependent on the temperature [41]. Since all DFT calculations are performed for $T = 0\,\text{K}$, the direct comparison between experimental and theoretical results are therefore not possible. As a result also the bulk modulus, a linear combination of second-order elastic constants, will be slightly higher at ambient conditions [41, 42].

The elastic stability of the α phase at equilibrium has been investigated by using the Born stability criterion [35], that requires that the eigenvalues of the stiffness tensor $\boldsymbol{C}$ are all positive. This has indeed been found for the α phase, the eigenvalues for C of the α phase were calculated and found to be positive. Therefore, we can conclude that the α phase at $T = 0\,\text{K}$ and $\boldsymbol{\sigma} = 0$ is elastically stable. The analogous discussion for the β phase was not possible due to the missing components in the stiffness tensor. However, all elastic moduli were higher for the α phase (see Table 3.16). This means that the α phase is harder than the β phase, if the hardness scales with the elastic moduli [37, 38]. The known phase transition of the β to the α phase [4] could possibly be the result of the lower bulk modulus. After obtaining the full stiffness tensor for the β phase, future calculations should be done to investigate the high-pressure behavior of both phases. The pressure-induced phase transition

at around 10 GPa from the α to the β phase should be investigated concerning the elastic stability with varying pressure. It has been proposed that the transition can be the result of shear stresses at the onset pressure [4]. In order to confirm this, the general Born stability criterion should be investigated with respect to the elastic stiffness tensor under load $\boldsymbol{B}$.

Bibliography

[1] Mannaerts J.P. Passlacki M., Hong M. *Appl. Phys. Lett.* **68**.

[2] Edwards D. D., Mason T. O., Goutenoire F. and Poeppelmeier K. R. *Appl. Phys. Lett. 70* **70**, (1997), 1706.

[3] Rustum R., V. G. Hill and E. F. Osborn, Polymorphism of Ga_2O_3 and the system Ga_2O_3—H_2O. *Journal of the American Chemical Society* **74** (3), (1952), 719–722.

[4] Kristina E. Lipinska-Kalita, Patricia E. Kalita, Oliver A. Hemmers and Thomas Hartmann. *Phys. Rev. B* **77**, (2008), 094123.

[5] S. Geller. *J. Chem. Phys.* **33**, (1960), 676.

[6] H. Wang, Y. He, W. Chen, Y. W. Zeng, K. Stahl, T. Kikegawa and J. Z. Jiang, High-pressure behavior of β-Ga_2O_3 nanocrystals. *Journal of Applied Physics* **107** (3).

[7] M. Marezio and J. P. Remeika, Bond lengths in the alpha Ga_2O_3 structure and the high-pressure phase of Ga_2-x$Fex O_3$. *J. Chem. Phys.* **46** (5), (1967), 1862–1865.

[8] R. Gross and A. Marx, Festkörperphysik. Oldenbourg Wissenschaftsverlag (2012).

[9] A. Gulans, S. Kontur, C. Meisenbichler, D. Nabok, P. Pavone, S. Rigamonti, S. Sagmeister, U. Werner and C. Draxl, exciting: a full-potential all-electron package implementing density-functional theory and many-body perturbation theory. *Journal of Physics: Condensed Matter* **26** (36), (2014), 363202.

[10] R. Golesorkhtabar, P. Pavone, J. Spitaler, P. Puschnig and C. Draxl, Elastic: A tool for calculating second-order elastic constants from first principles. *Computer Physics Communications* **184** (8), (2013), 1861 – 1873.

[11] S. Timoshenko, Theory of Elasticity. McGraw-Hill (1951).

[12] Giustino F., Materials Modelling using Density Functional Theory: Properties and Predictions. Oxford University Press (2014).

[13] D. C. Wallace, Thermodynamics of Crystals. Wiley (1972).

[14] L. D. Landau and E. M. Lifschitz, Theory of Elasticity. Elsevier (1986).

[15] W. Nolting, Grundkurs Theoretische Physik 1:. Grundkurs: Theoretische Physik, Springer (2004).

[16] W. Voigt, Lehrbuch der Kristallphysik: mit Ausschluss der Kristalloptik. J.W. Edwards (1928).

[17] Z. Angew A. Reuss. *Math. Mech.* **9**, (1929), 49–58.

[18] R. Hill, The elastic behaviour of a crystalline aggregate. *Proc. Phys. Soc. A* **65**, (1952), 349.

[19] R. Hill, Elastic properties of reinforced solids: some theoretical principles. *J. Mech. Phys. Solids* **11**, (1963), 357.

[20] M. Born and R. Oppenheimer, Zur Quantentheorie der Molekeln. *Annalen der Physik* **389** (20), (1927), 457–484.

[21] P. Hohenberg and W. Kohn, Inhomogeneous electron gas. *Phys. Rev.* **136**, (1964), B864–B871.

[22] W. Kohn and L. J. Sham, Self-consistent equations including exchange and correlation effects. *Phys. Rev.* **140**, (1965), A1133–A1138.

[23] A. Zunger J. P. Perdew. *Phys. Rev. B* **23**, (1984), 5048–5079.

[24] J. P. Perdew, K. Burke and M. Ernzerhof. *Phys. Rev. Lett.* **77**, (1996), 3865–3868.

[25] John P. Perdew, Adrienn Ruzsinszky, Gábor I. Csonka, Oleg A. Vydrov, Gustavo E. Scuseria, Lucian A. Constantin, Xiaolan Zhou and Kieron Burke, Restoring the density-gradient expansion for exchange in solids and surfaces. *Phys. Rev. Lett.* **100**, (2008), 136406.

[26] O. Krogh Andersen, Linear methods in band theory. *Phys. Rev. B* **12**, (1975), 3060–3083.

[27] E. Sjöstedt, L. Nordström and D. J. Singh, An alternative way of linearizing the augmented plane-wave method. *Solid State Communications* **114** (1), (2000), 15 – 20.

[28] Francis Birch, Finite elastic strain of cubic crystals. *Phys. Rev.* **71**, (1947), 809–824.

[29] M. Râsander and M. A. Moram, On the accuracy of commonly used density functional approximations in determining the elastic constants of insulators and semiconductors. *J. Chem. Phys.* **143** (14), 144104.

[30] Richard H. Byrd, Peihuang Lu, Jorge Nocedal and Ciyou Zhu, A limited memory algorithm for bound constrained optimization. *SIAM Journal on Scientific Computing* **16** (5), (1995), 1190–1208.

[31] C. Kittel, Introduction to Solid State Physics. Wiley (2004).

[32] Haiying He, Roberto Orlando, Miguel A. Blanco, Ravindra Pandey, Emilie Amzallag, Isabelle Baraille and Michel Rérat, First-principles study of the structural, electronic, and optical properties of Ga_2O_3 in its monoclinic and hexagonal phases. *Phys. Rev. B* **74**, (2006), 195123.

[33] F. Litimein, D. Rached, R. Khenata and H. Baltache, FPLAPW study of the structural, electronic, and optical properties of Ga_2O_3: Monoclinic and hexagonal phases. *Journal of Alloys and Compounds* **488** (1), (2009), 148 – 156.

[34] S Yoshioka, H Hayashi, A Kuwabara, F Oba, K Matsunaga and I Tanaka, Structures and energetics of Ga_2O_3 polymorphs. *Journal of Physics: Condensed Matter* **19** (34), (2007), 346211.

[35] M. Born, On the stability of crystal lattices. i. *Mathematical Proceedings of the Cambridge Philosophical Society* **36**, (1940), 160–172.

[36] Félix Mouhat and François-Xavier Coudert, Necessary and sufficient elastic stability conditions in various crystal systems. *Phys. Rev. B* **90**, (2014), 224104.

[37] Hsiu-Ying Chung, Michelle B. Weinberger, Jenn-Ming Yang, Sarah H. Tolbert and Richard B. Kaner. *Applied Physics Letters* **92** (26).

[38] Léger Haines J., Bocquillon G. *Annu. Rev. Mater. Res.* **31**.

[39] Göran Grimvall, Blanka Magyari-Köpe, Vidvuds Ozoliņš and Kristin A. Persson, Lattice instabilities in metallic elements. *Rev. Mod. Phys.* **84**, (2012), 945–986.

[40] P. Haas, F. Tran and P. Blaha, Calculation of the lattice constant of solids with semilocal functionals. *Phys. Rev. B* **79**, (2009), 085104.

[41] M. Born and K. Huang, Dynamical Theory of Crystal Lattices. Clarendon Press (1998).

[42] Y. P. Varshni, Temperature dependence of the elastic constants. *Phys. Rev. B* **2**, (1970), 3952–3958.

Appendix A

Listing 1 : Species file for Gallium

```
<?xml version="1.0" encoding="UTF-8"?>
<spdb xsi:noNamespaceSchemaLocation="../../xml/species.xsd"
   xmlns:xsi="http://www.w3.org/2001/XMLSchema-instance">
  <sp chemicalSymbol="Ga" name="gallium" z="-31.0000"
  mass="127097.2538">
    <muffinTin rmin="0.100000E-04" radius="1.9000" rinf="28.4824"
       radialmeshPoints="400"/>
    <atomicState n="1" l="0" kappa="1" occ="2.00000" core="true"/>
    <atomicState n="2" l="0" kappa="1" occ="2.00000" core="true"/>
    <atomicState n="2" l="1" kappa="1" occ="2.00000" core="true"/>
    <atomicState n="2" l="1" kappa="2" occ="4.00000" core="true"/>
    <atomicState n="3" l="0" kappa="1" occ="2.00000" core="false"/>
    <atomicState n="3" l="1" kappa="1" occ="2.00000" core="false"/>
    <atomicState n="3" l="1" kappa="2" occ="4.00000" core="false"/>
    <atomicState n="3" l="2" kappa="2" occ="4.00000" core="false"/>
    <atomicState n="3" l="2" kappa="3" occ="6.00000" core="false"/>
    <atomicState n="4" l="0" kappa="1" occ="2.00000" core="false"/>
    <atomicState n="4" l="1" kappa="1" occ="1.00000" core="false"/>
    <basis>
      <default type="lapw" trialEnergy="0.1500" searchE="false"/>

      <custom l="0" type="apw+lo" trialEnergy="0.1500"
      searchE="false"/>
      <lo l="0">
        <wf matchingOrder="0" trialEnergy="0.1500"
        searchE="false"/>
        <wf matchingOrder="0" trialEnergy="-5.02" searchE="false"/>
      </lo>
      <lo l="0">
        <wf matchingOrder="0" trialEnergy="-5.02" searchE="false"/>
        <wf matchingOrder="1" trialEnergy="-5.02" searchE="false"/>
      </lo>

      <custom l="1" type="apw+lo" trialEnergy="0.1500"
      searchE="false"/>
      <lo l="1">
        <wf matchingOrder="0" trialEnergy="0.1500"
        searchE="false"/>
        <wf matchingOrder="0" trialEnergy="-3.20" searchE="false"/>
      </lo>
     <lo l="1">
        <wf matchingOrder="0" trialEnergy="-3.20" searchE="false"/>
        <wf matchingOrder="1" trialEnergy="-3.20" searchE="false"/>
      </lo>
```

```
      <custom l="2" type="apw+lo" trialEnergy="-0.30"
      searchE="false"/>
     <lo l="2">
        <wf matchingOrder="0" trialEnergy="-0.30" searchE="false"/>
        <wf matchingOrder="2" trialEnergy="-0.30" searchE="false"/>
      </lo>

    </basis>
  </sp>
</spdb>

<!—->
```

Listing 2 : Species file for Oxygen

```
<?xml version="1.0" encoding="UTF-8"?>
<spdb xsi:noNamespaceSchemaLocation="../../xml/species.xsd"
   xmlns:xsi="http://www.w3.org/2001/XMLSchema-instance">
  <sp chemicalSymbol="O" name="oxygen" z="-8.00000"
  mass="29165.12203">
    <muffinTin rmin="0.100000E-04" radius="1.5000" rinf="17.0873"
       radialmeshPoints="300"/>
    <atomicState n="1" l="0" kappa="1" occ="2.00000" core="true"/>
    <atomicState n="2" l="0" kappa="1" occ="2.00000" core="false"/>
    <atomicState n="2" l="1" kappa="1" occ="2.00000" core="false"/>
    <atomicState n="2" l="1" kappa="2" occ="2.00000" core="false"/>
    <basis>
      <default type="lapw" trialEnergy="0.1500" searchE="false"/>

      <custom l="0" type="apw+lo" trialEnergy="-0.50"
      searchE="false"/>
      <lo l="0">
        <wf matchingOrder="0" trialEnergy="-0.50" searchE="false"/>
        <wf matchingOrder="2" trialEnergy="-0.50" searchE="false"/>
      </lo>

      <custom l="1" type="apw+lo" trialEnergy="0.1500"
      searchE="false"/>
      <lo l="1">
        <wf matchingOrder="0" trialEnergy="0.1500"
        searchE="false"/>
        <wf matchingOrder="2" trialEnergy="0.1500"
        searchE="false"/>
      </lo>

      <custom l="2" type="apw+lo" trialEnergy="0.1500"
      searchE="false"/>
      <lo l="2">
        <wf matchingOrder="0" trialEnergy="0.1500"
        searchE="false"/>
        <wf matchingOrder="2" trialEnergy="0.1500"
        searchE="false"/>
      </lo>

    </basis>
  </sp>
</spdb>

<!—->
```

Appendix B

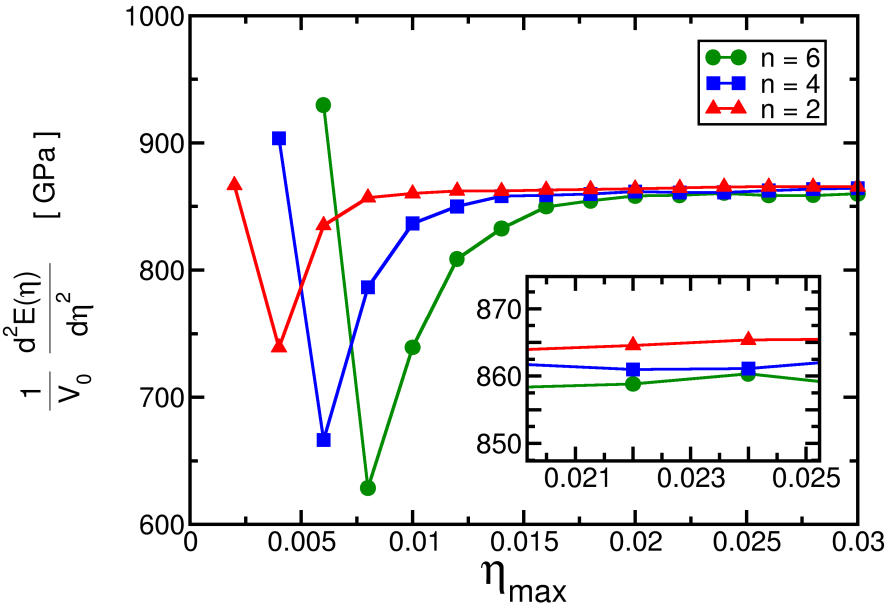

(a) $\boldsymbol{\eta} = (0, \eta, -\eta, 0, 0, 0)$

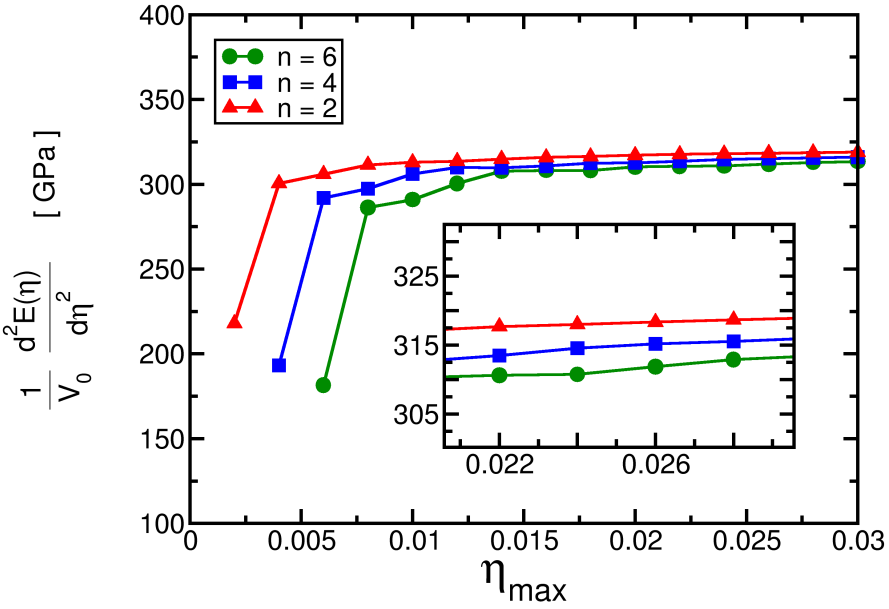

(b) $\boldsymbol{\eta} = (\eta, -\eta, 0, 0, 0, 0)$

Figure 16: Energy derivative-vs.-strain curve as obtained from total-energy calculations (dots) and a corresponding polynomial fit of order n (solid line) for the β phase of Ga_2O_3, with n the order of the polynomial. The applied Lagrangian strain tensor is specified in (a) and (b).

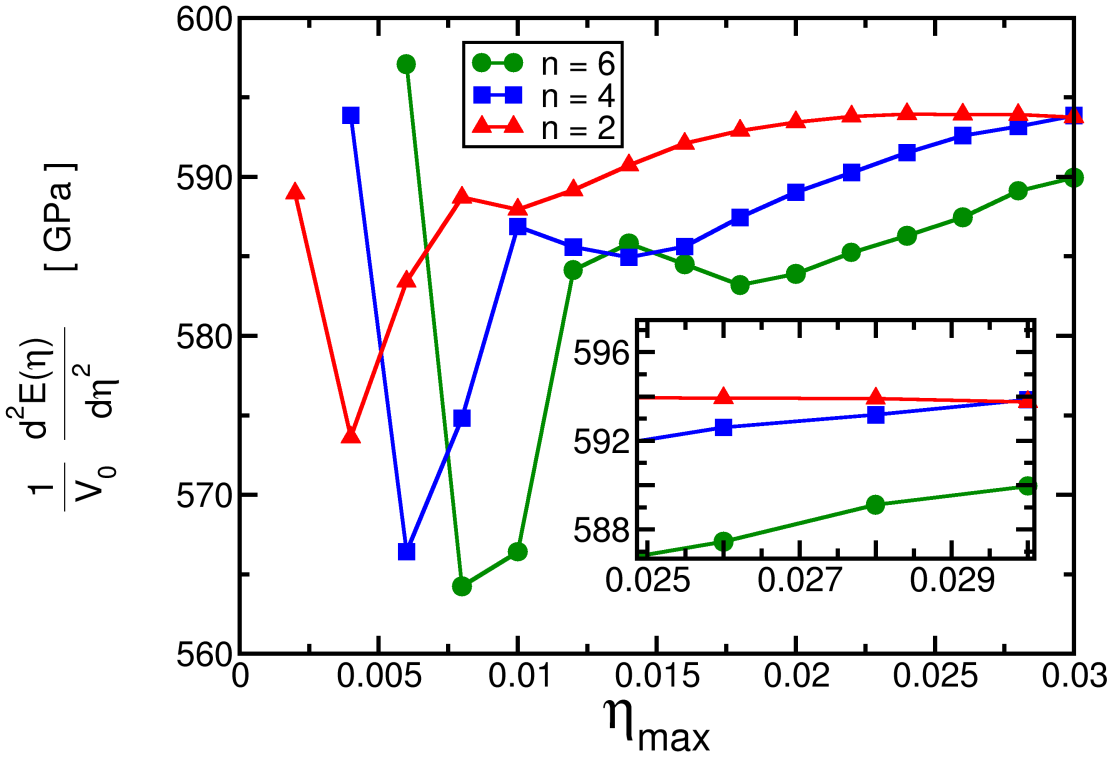

(a) $\boldsymbol{\eta} = (\eta, 0, 0, 0, 0, 2\eta)$

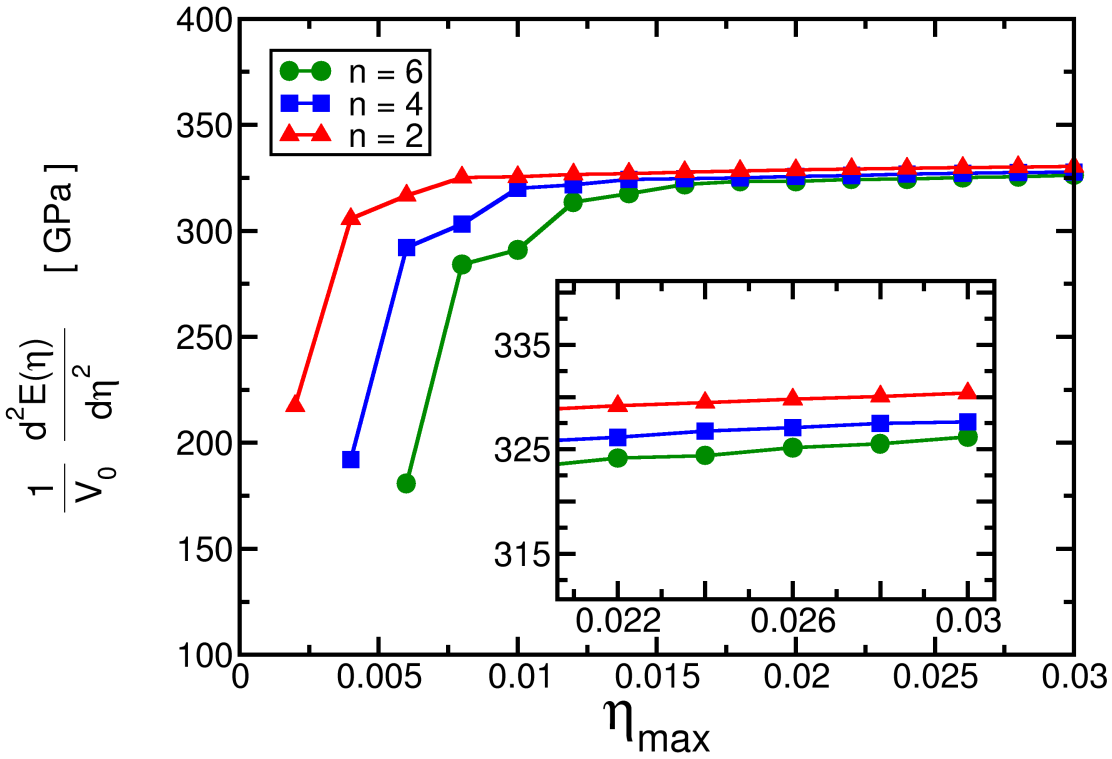

(b) $\boldsymbol{\eta} = (0, \eta, 0, 0, 0, 0)$

Figure 17: Same as Fig. 16 with the strain tensor specified in (a) and (b).

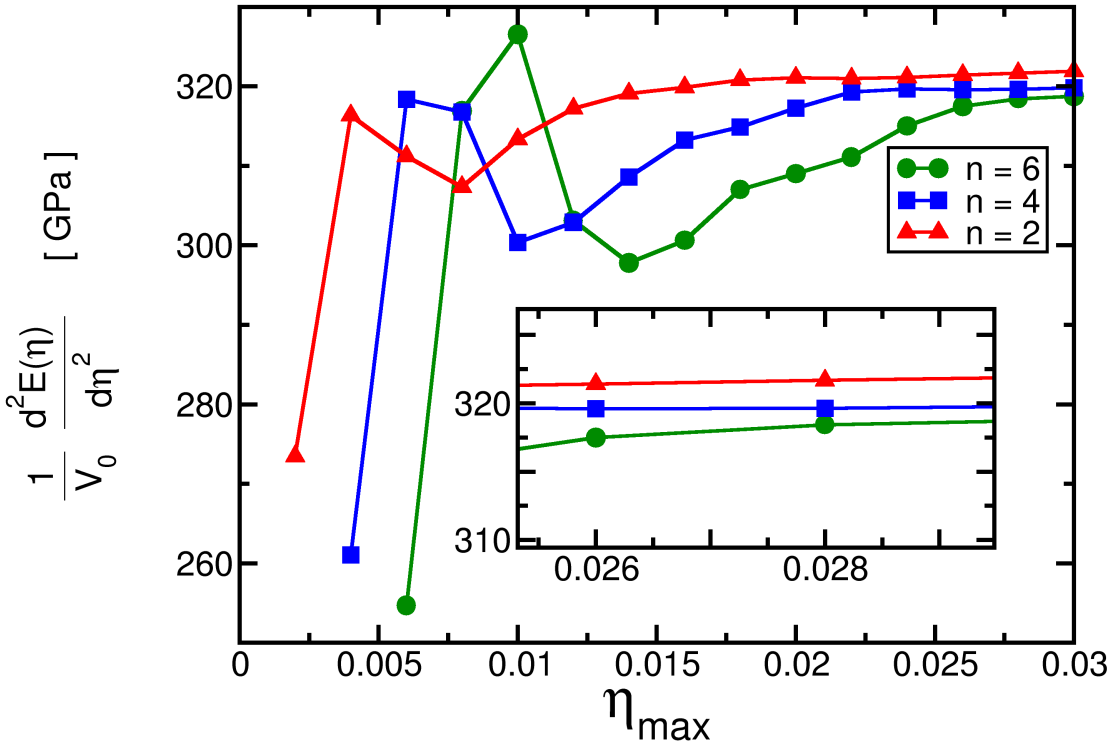

(a) $\boldsymbol{\eta} = (0, 0, \eta, 0, 0, 0)$

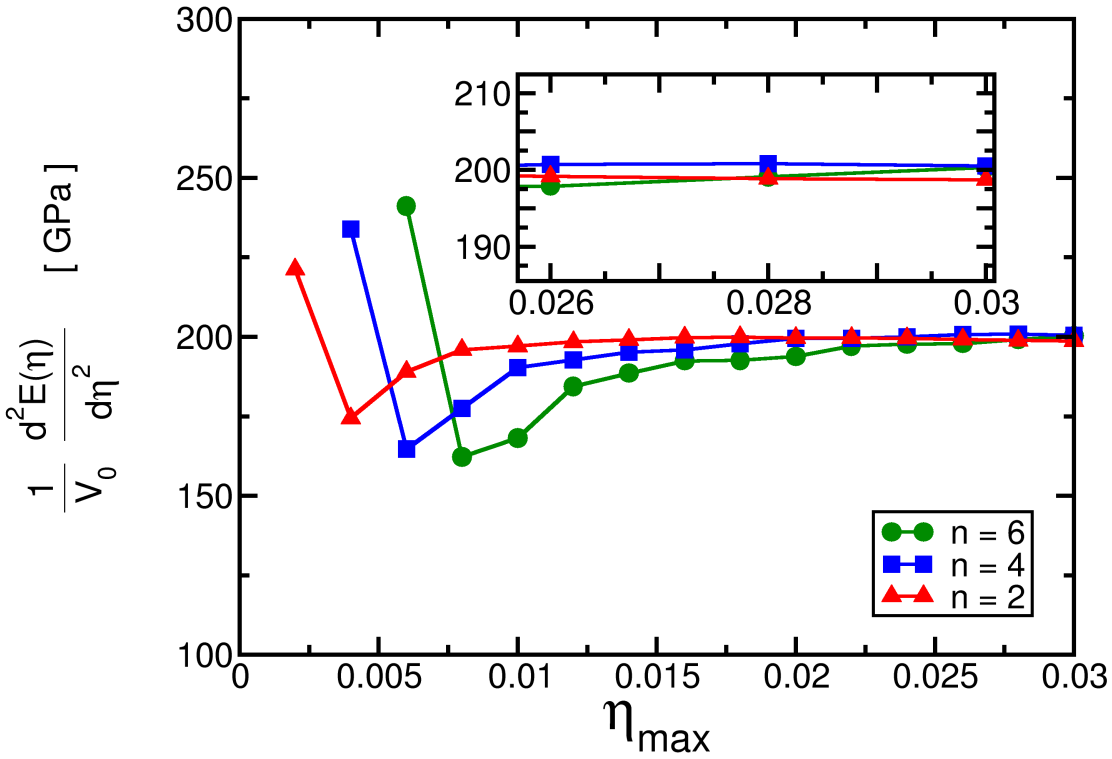

(b) $\boldsymbol{\eta} = (0, 0, 0, 2\eta, 0, 0)$

Figure 18: Same as Fig. 16 with the strain tensor specified in (a) and (b).

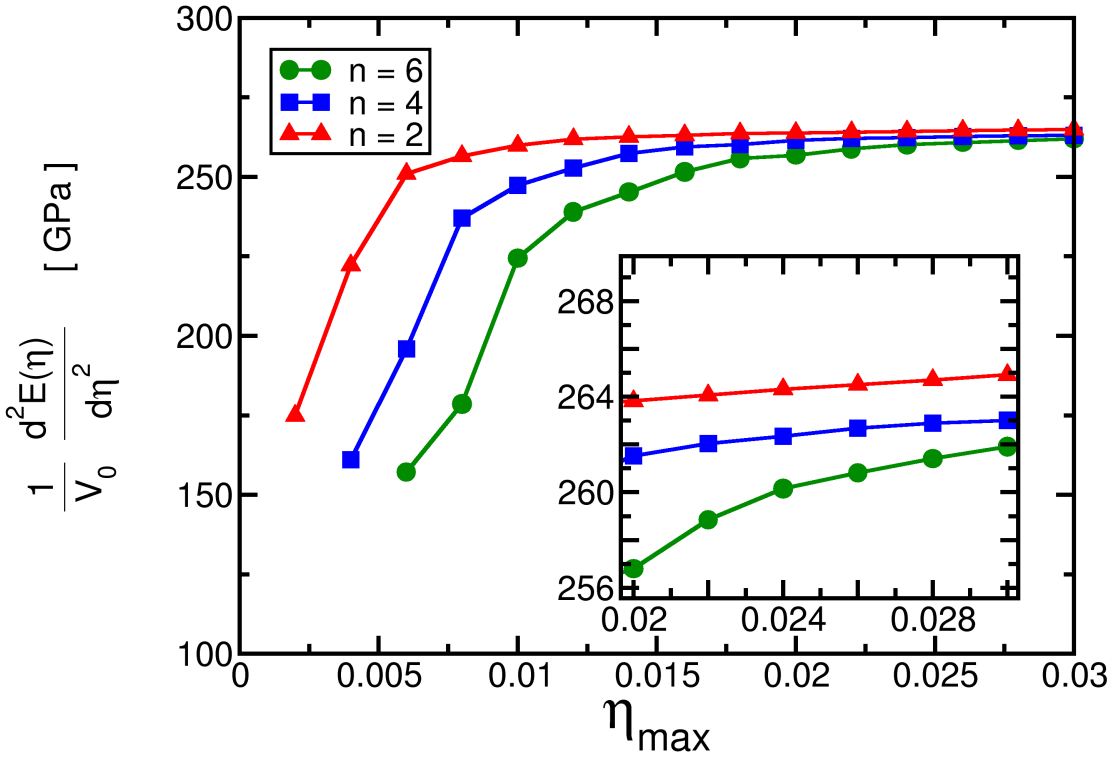

(a) $\boldsymbol{\eta} = (0, 0, 0, 0, 2\eta, 0)$

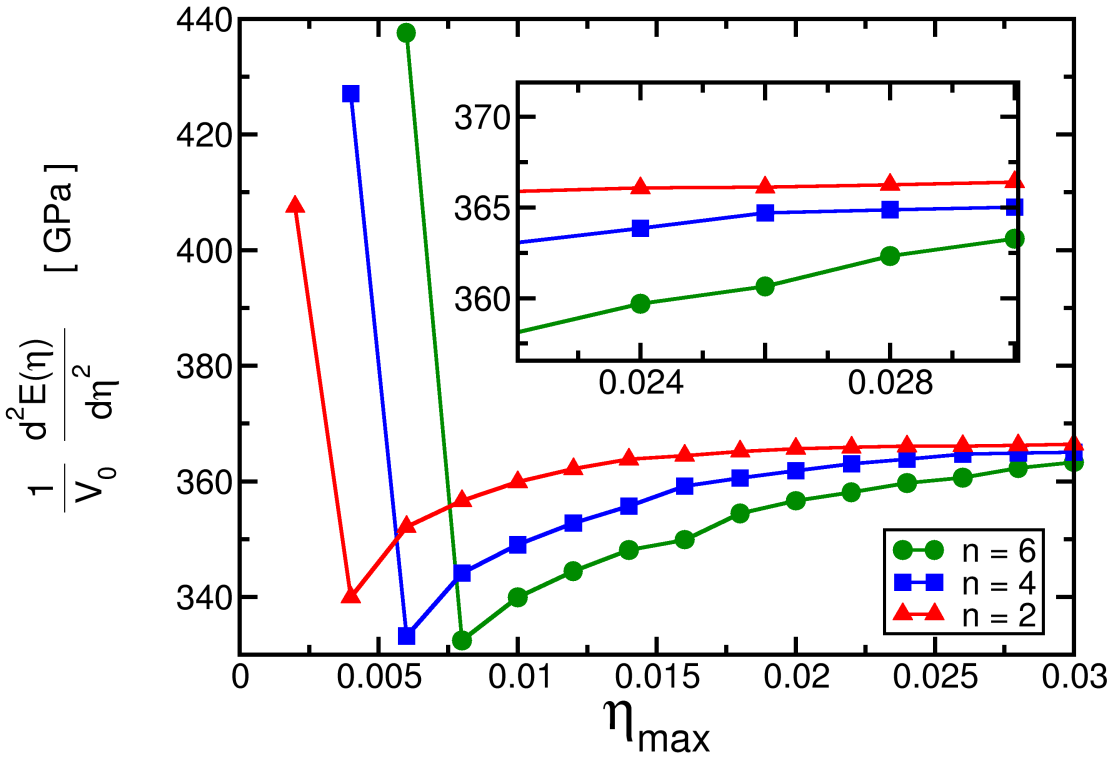

(b) $\boldsymbol{\eta} = (0, 0, 0, 0, 0, 2\eta)$

Figure 19: Same as Fig. 16 with the strain tensor specified in (a) and (b).

Selbstständigkeitserklärung

Hiermit versichere ich, Konstantin Lion, dass ich meine Abschlussarbeit selbstständig verfasst und keine anderen als die angegebenen Quellen und Hilfsmittel benutzt habe.

.....
(Datum und Unterschrift)